STATISTICAL PROPERTIES OF THE LARGE SCALE STRUCTURES:

# CLUSTERING

**For a review on structure formation:**
https://sites.astro.caltech.edu/~george/ay127/kamionkowski-perturbations-notes.pdf
https://people.ast.cam.ac.uk/~pettini/Intro%20 Cosmology/Lecture14.pdf
**For a review on BAO:** https://arxiv.org/pdf/0910.5224.pdf
**For a review on RSD:** https://arxiv.org/pdf/astro-ph/9708102.pdf

# EVOLUTION OF DENSITY PERTURBATIONS

**Inflation generates primordial perturbations through the amplification of quantum fluctuations, which are stretched to astrophysical scales by the rapid expansion.**

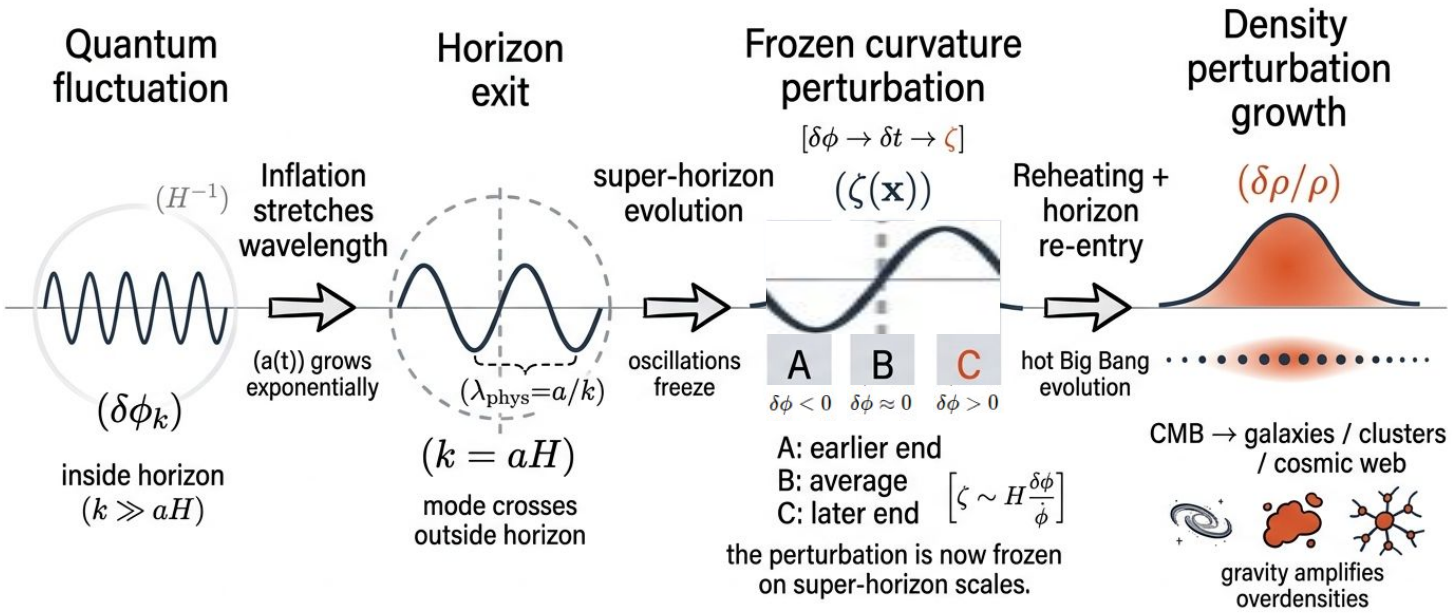


$$[\delta\phi_k \longrightarrow \zeta_k \longrightarrow \delta_m(\mathbf{x})]$$

Inflation stretches microscopic quantum fluctuations to super-horizon scales, where they freeze as curvature perturbations and later seed the growth of cosmic structure.

# EVOLUTION OF DENSITY PERTURBATIONS

**The simplest models of inflation predict that the initial fluctuations constitute a Gaussian random field, with an almost purely adiabatic primordial perturbations with a near scale-invariant power spectrum. In these models the primordial power spectrum is often described in terms of a spectral index $n_s$ and an amplitude of the perturbations $A_s$ as ($k_p$ = 0.05 Mpc$^{-1}$ = pivot scale ):**

$$P(k) = A_s \left( \frac{k}{k_p} \right)^{n_s}$$

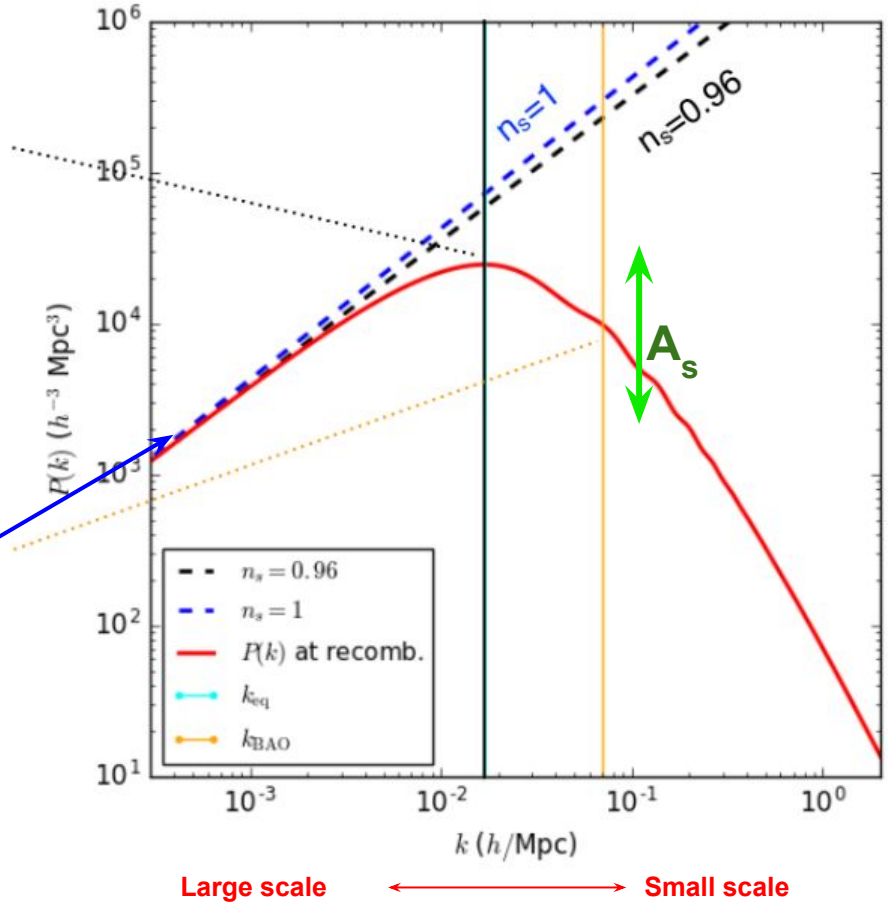

# EVOLUTION OF DENSITY PERTURBATIONS

**After the perturbations are created in the early Universe, they undergo a complex evolution which depends on the theory of gravity (GR), and the expansion history of the Universe.**

- **Gravity is the dominant force that moves matter on the largest scales.**
- **The dark matter, which constitutes ~ 5/6 of the nonrelativistic matter in the Universe, is composed of “cold dark matter”, pressureless matter that interacts with everything else only gravitationally.**

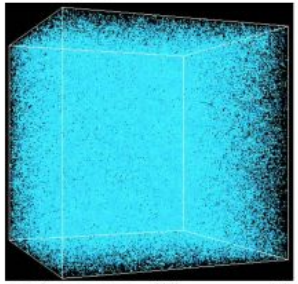
Universe 120 million years old

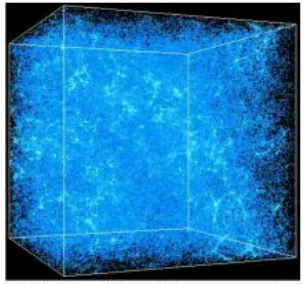
Universe 490 million years old

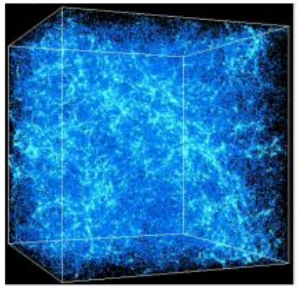
Universe 1.2 billion years old

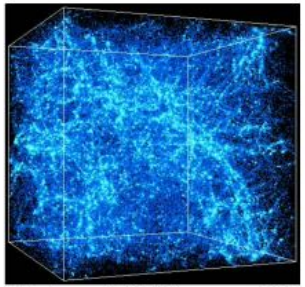
Universe 2.2 billion years old

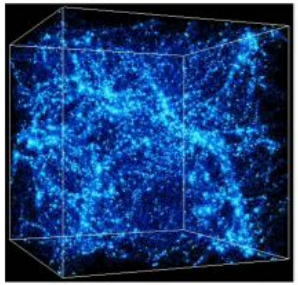
Universe 6.0 billion years old

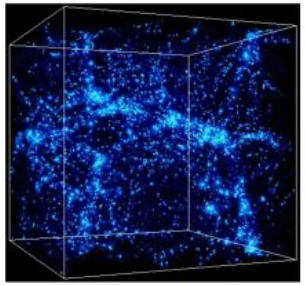
Universe 13.7 billion years old

# EVOLUTION OF DENSITY PERTURBATIONS

- **Overdensity field:**

$$\delta(\mathbf{x}) \equiv \frac{\rho(\mathbf{x}) - \langle\rho\rangle}{\langle\rho\rangle}$$

**For CDM model:**

| | $z > z_{eq}$ (RD) | $z < z_{eq}$ (MD) |
|---|---|---|
| $R > R_H$ | $\delta_r \propto \delta_m \propto a^2$ | $\delta_r \propto \delta_m \propto a$ |
| $R < R_H$ | $\delta_{cdm} \sim const$<br>$\delta_{b+\gamma}$ *oscillations* | $\delta_{cdm} \propto a$<br>$z < z_{rec}$: $\delta_b \to \delta_{cdm}$ |

**Matter-radiation equality**

$$\frac{\rho_m(a_{eq})}{\rho_r(a_{eq})} = 1$$

$$1 + z_{eq} = \frac{a_0}{a_{eq}} \simeq 3250$$

**Hubble radius**

$$R_H(t) = \frac{c}{H(t)} \sim c\,t$$

# EVOLUTION OF DENSITY PERTURBATIONS

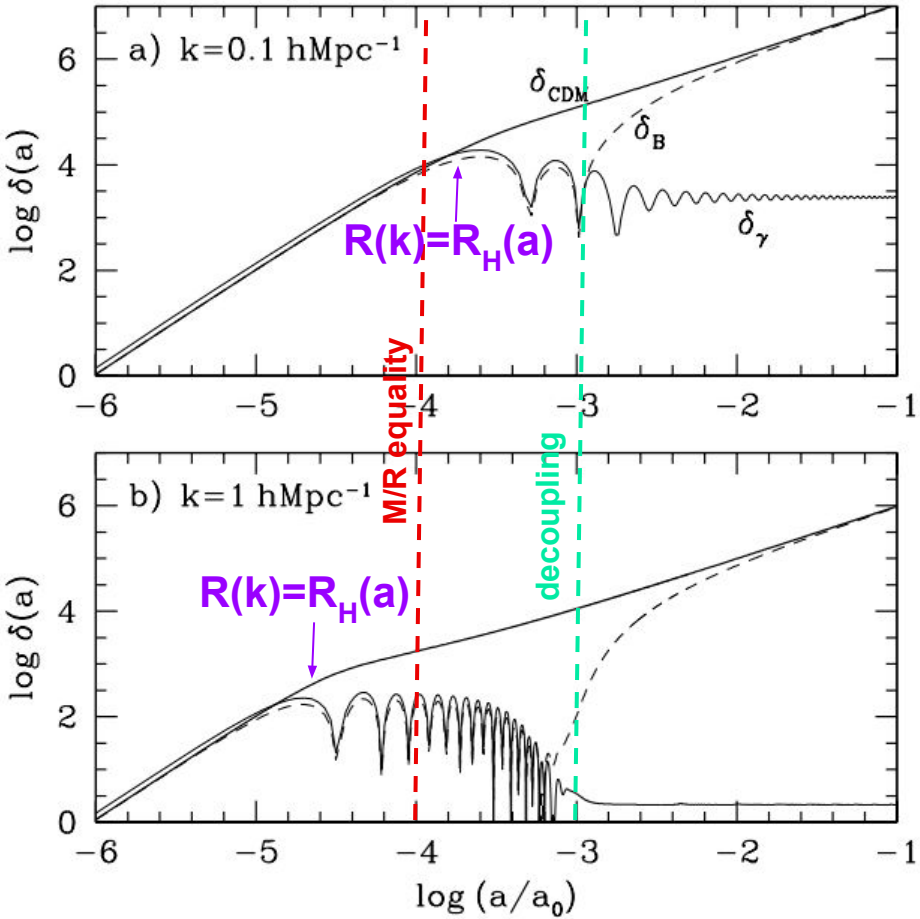


The evolution of adiabatic perturbations in a CDM universe with $\Omega_{\mathrm{m},0} = 1$, $\Omega_{\mathrm{B},0} = 0.05$, $h = 0.5$.
The scale factor is normalized at the present time.
Decoupling: $a \sim 10^{-3}$
Matter/radiation equality: $a \sim 10^{-4}$

Note: Since these modes enters horizon after (k=0.1) or just before (k=1) matter-radiation equality, there is no Meszaros effect ( $\delta_{\mathrm{cdm}}$ ~ cost)

# EVOLUTION OF DENSITY PERTURBATIONS

**The primordial power spectrum of density fluctuations gets "processed" by the growth of density perturbations:**

$$P(k,z) = P_{\rm primordial}(k)T^2(k,z)$$

**where the transfer function T(k) takes into account the effects of gravitational amplification of density perturbation mode of wavelength *k***

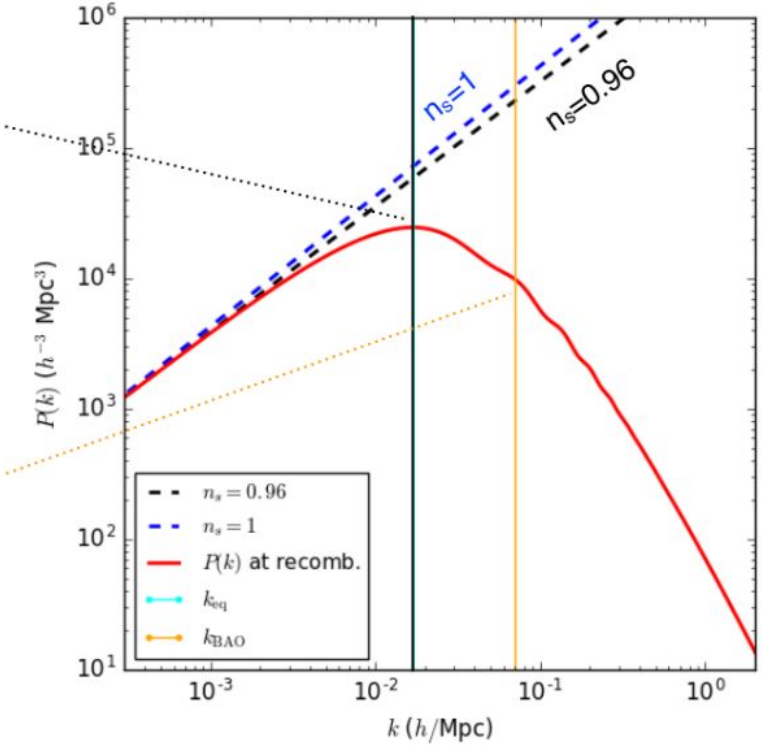

# EVOLUTION OF DENSITY PERTURBATIONS

**The primordial power spectrum of density fluctuations gets "processed" by the growth of density perturbations:**

$$P(k,z) = P_{\rm primordial}(k)T^2(k,z)$$

**where the transfer function T(k) takes into account the effects of gravitational amplification of density perturbation mode of wavelength *k***

**Transfer function for different components**

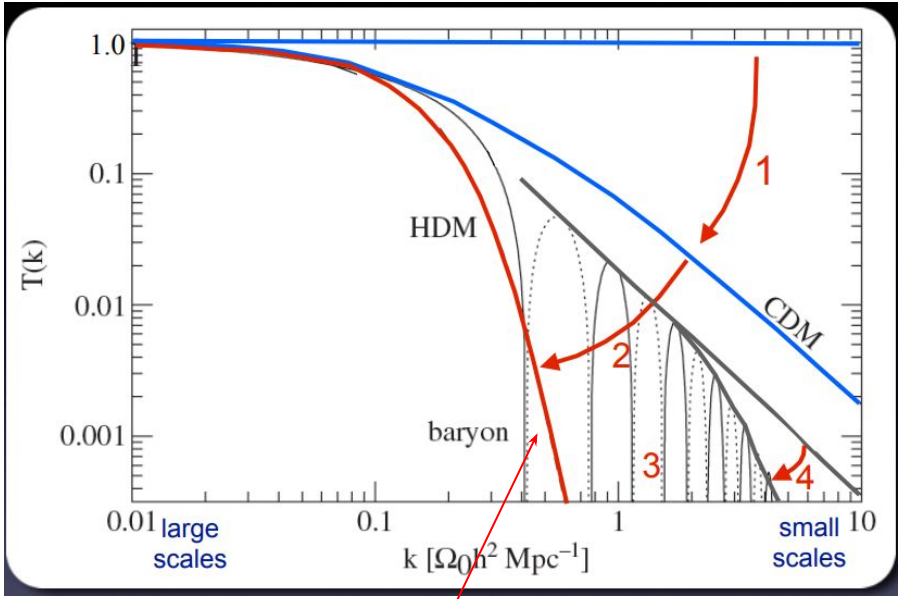


**Note: The thermal velocity of DM particles determines the free streaming length below which structure formation is suppressed (free-streaming damping)**

# SIDE NOTE: HOT, WARM AND COLD DARK MATTER

**Free-streaming cut-off scale:**

$$k_{\rm FS} \sim 15.6 \frac{h}{\rm Mpc} \left(\frac{m_{\rm WDM}}{1{\rm keV}}\right)^{4/3} \left(\frac{0.12}{\Omega_{\rm DM} h^2}\right)^{1/3}$$

**Cosmic Relics**

**Non-thermal Relics**

not produced in thermal equilibrium (TE) with rest of Universe.

e.g., axions (FDM), monopoles, cosmic strings

**Thermal Relics**

are held in TE with other components of Universe until they `decouple', which happens when interaction rate $\Gamma = n\langle\sigma v\rangle$ drops below expansion rate $H(a)$

**Hot Dark Matter**

particles are still relativistic at decoupling, i.e., $3k_{\rm B}T_{\rm d} > m_{\rm X}c^2$

e.g., massive neutrinos

**Cold Dark Matter**

particles are non-relativistic at decoupling i.e., $3k_{\rm B}T_{\rm d} < m_{\rm X}c^2$

e.g., WIMPS

**Warm Dark Matter**

E.g. keV sterile neutrino

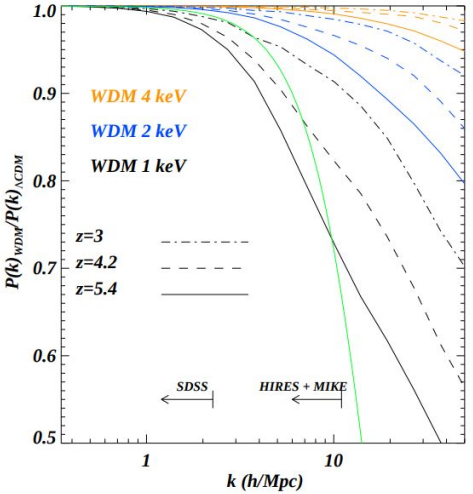

# EVOLUTION OF DENSITY PERTURBATIONS

**Transfer function (CDM):**

$$T(k) \simeq \begin{cases} 1, & k \lesssim k_{\rm eq}, \\ (k/k_{\rm eq})^{-2}, & k \gtrsim k_{\rm eq}, \end{cases}$$

**The characteristic length scale is the horizon-size at matter-radiation equality, $k_{eq} = 2\pi(ct_{eq})^{-1} \propto \Omega_{m,0}h^2$: before $t_{eq}$, below the horizon, dark matter fluctuations cannot growth.**

**Thus, if $P_{primordial}(k) \propto k^n$ , the processed power spectrum is:**

- **$P(k) \propto k^n$ for $k \ll k_{eq}$ (above the horizon)**
- **$P(k) \propto k^{n-4}$ for $k \gg keq$ (below the horizon)**

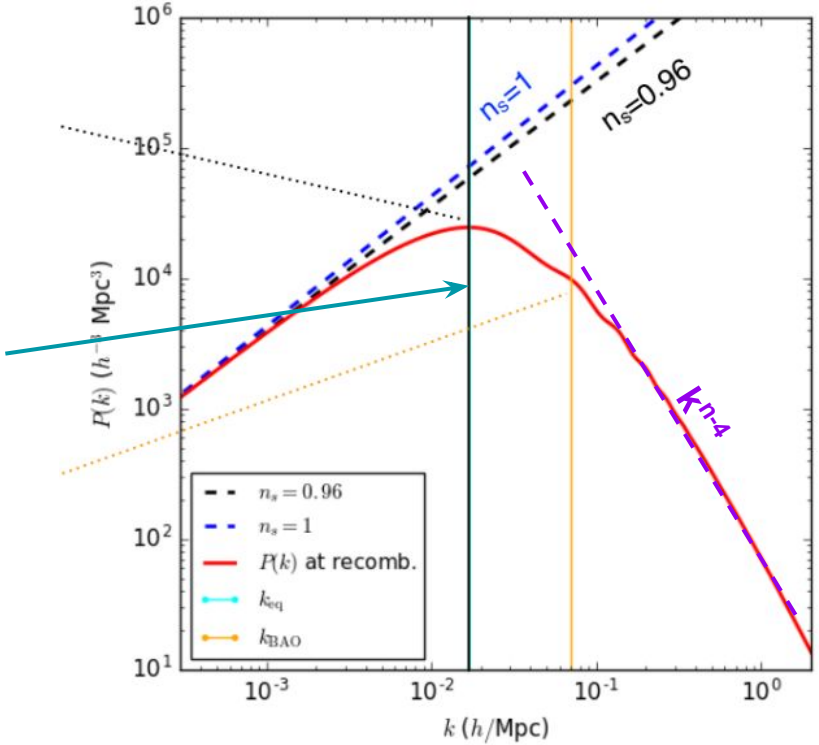

# EVOLUTION OF DENSITY PERTURBATIONS

**Baryonic Acoustic Oscillations**:

**In the early, high-temperature Universe, baryons and photons were tightly coupled by Compton scattering, (photon-baryon fluid); the competing forces of radiation pressure and gravity set up oscillations in the photon-baryon fluid. As the Universe expands and cools down, atoms form (Recombination) and the interaction rate between baryons and photons decreases: photons begin to free-stream, leaving baryons in a shell with a radius approximately equal to the sound horizon at the time of decoupling. From that moment on, only the gravitational interaction between dark matter and baryonic matter remains. This characteristic radius is therefore imprinted as an overdensity and the power spectrum have an excess of power on this scale.**

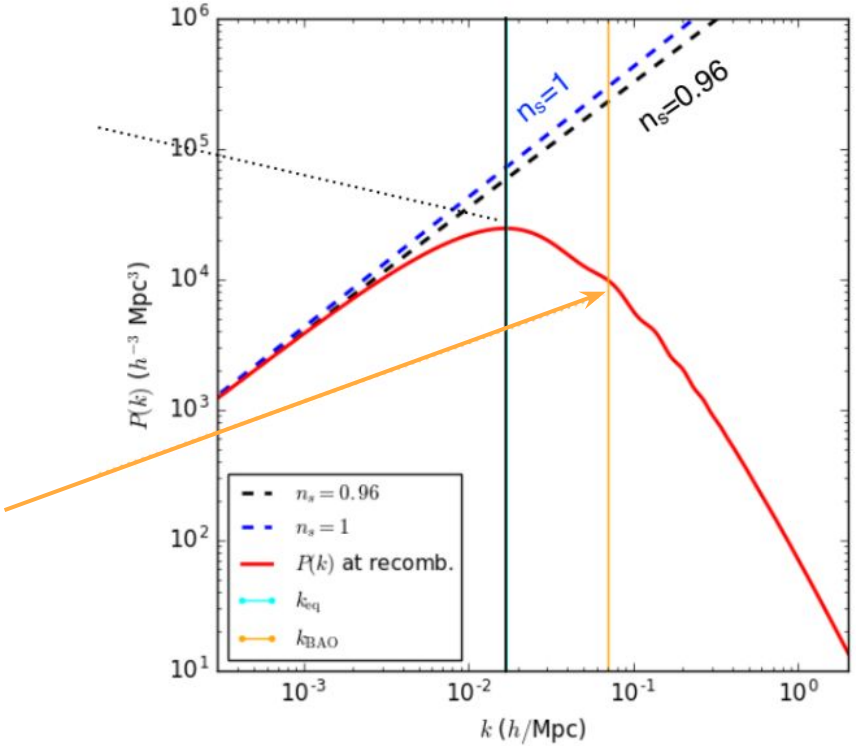

# TWO-POINT CORRELATION FUNCTION

**The most commonly used quantitative measure of large scale structure is the two-point correlation function. The two-point correlation function, ξ(*r*), is the excess probability (compared to an unclustered Poisson distribution) of finding two tracers of the matter density field (e.g. galaxies) separated by a distance *r* from each other:**

$$dP = n(1 + \xi(r))dV$$

**Where *n* is the mean number density of the tracer in question.**

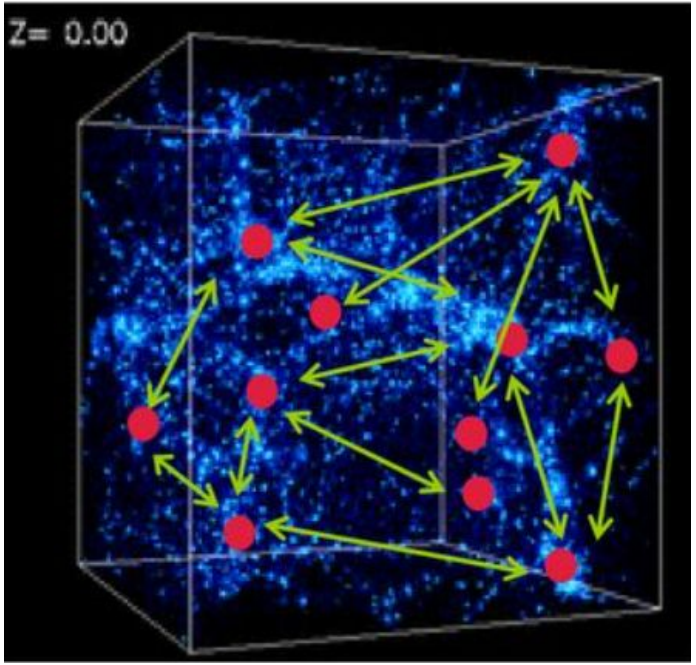


**2 pt. Correlation Function Estimators:**

$$\hat{\xi}(r) = \frac{DD(r) - RR(r)}{RR(r)}$$ (Peebles & Hauser, 1974)

$$\hat{\xi}(r) = \frac{DD(r) - 2DR(r) + RR(r)}{RR(r)}$$ (Landy & Szalay, 1993)

# 2PT CORRELATION FUNCTION

**E.g.: the data points in Figure are drawn from distributions with equal densities, but different clustering properties.**

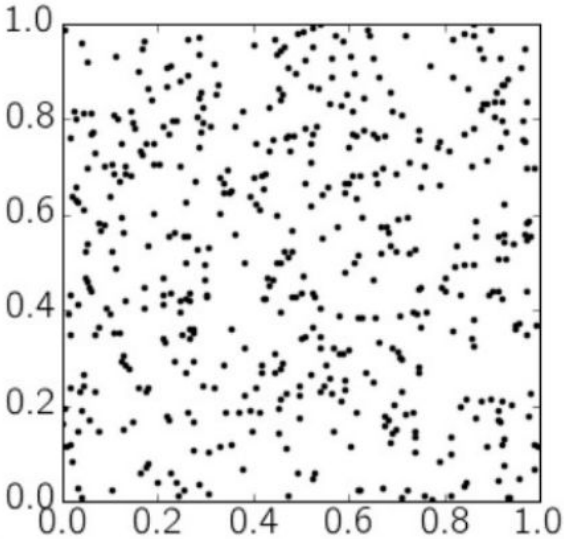


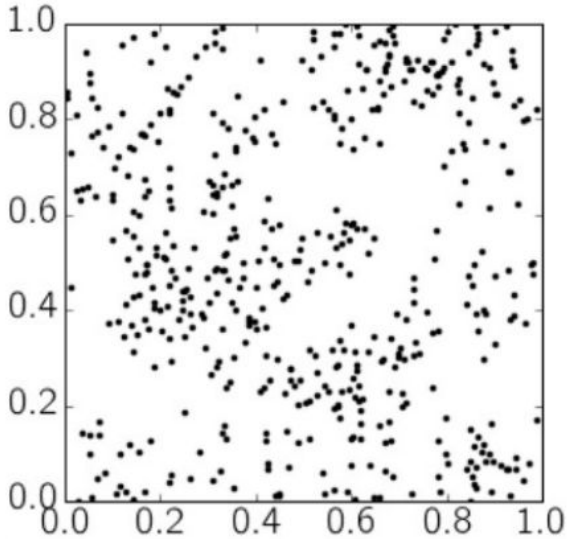

# 2PT CORRELATION FUNCTION

**E.g.: the data points in Figure are drawn from distributions with equal densities, but different clustering properties.**

**Using the two-point correlation function we can characterize the different clustering properties between the distributions.**

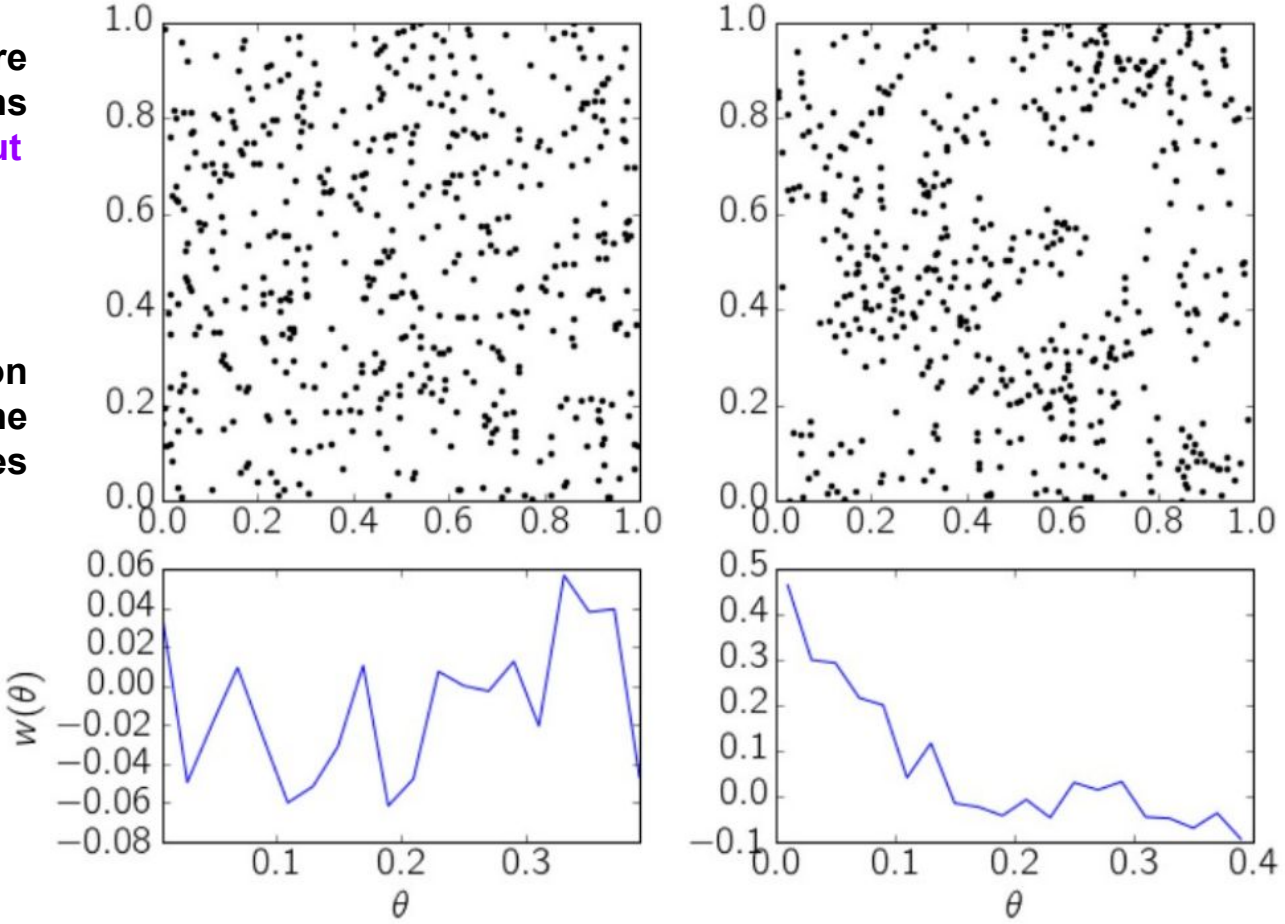

# 2PT CORRELATION FUNCTION

**Assuming the universe is isotropic, the correlation function is a function of a *scalar* distance. The two-point correlation function can then be written as**

$$\xi(\vec{r}) := \langle \delta(\vec{x})\delta(\vec{x}+\vec{r}) \rangle$$

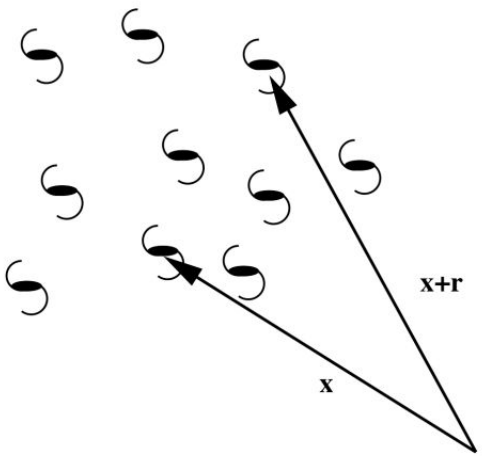


**The 2PCF is closely connected to the power spectrum; They form a Fourier transform pair:**

$$\xi(\vec{r}) = \frac{1}{(2\pi)^3} \int \mathrm{d}^3 k P(\vec{k}) e^{i\vec{k}\cdot\vec{r}},$$

$$P(\vec{k}) = \int \mathrm{d}^3 r \xi(\vec{r}) e^{-i\vec{k}\cdot\vec{r}},$$

**A Gaussian random field is completely specified by either the two-point correlation function, or, equivalently, the power spectrum P(k)!**

# LINEAR 2PT CF AND POWER SPECTRUM

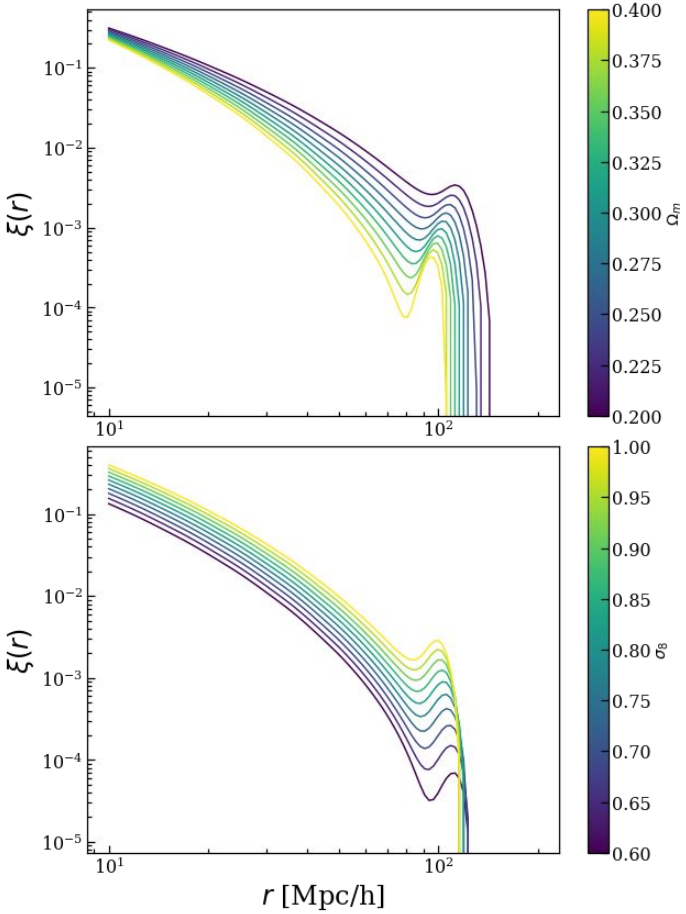


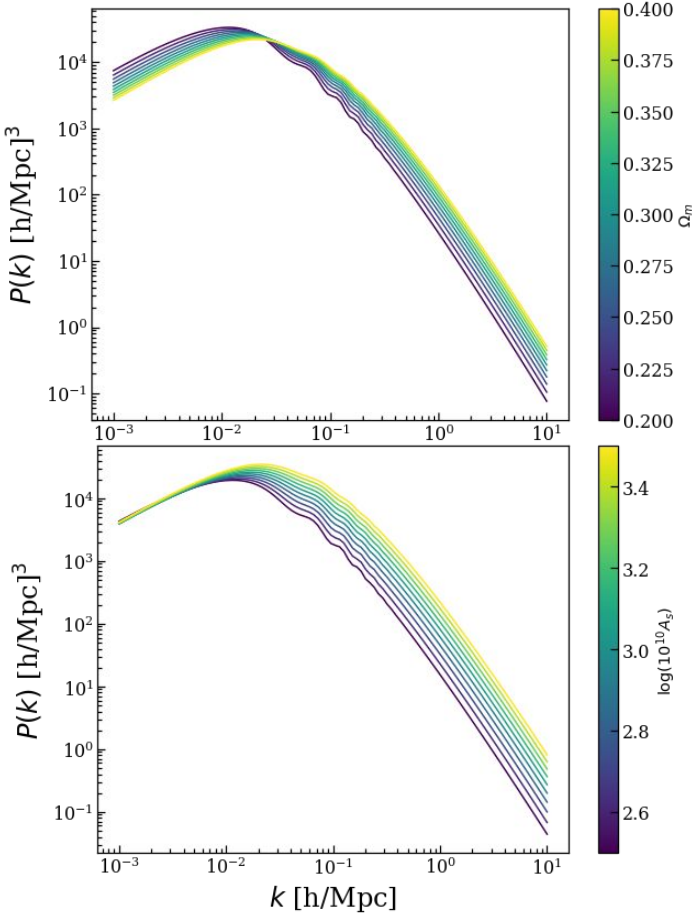

# NON-LINEAR EVOLUTION

In the linear regime ($\delta$<<1 ) we can calculate the evolution of a density field using linear perturbation theory:

$$P_{Lin}(k,z) = D(z)\, P_{Lin}(k,z=0)$$

In the non-linear regime ($\delta$>1) perturbation theory is no longer valid. ***Modes start to couple*** to each other, and one can no longer describe the evolution of the density field with a simple growth rate: in general, no analytic solutions exist and we must rely on simulations.

**Because of this mode-coupling, the density field loses its Gaussian properties, i.e., in the non-linear regime, we no longer have a Gaussian random field. Hence, higher-order moments are required to completely specify the density field.**

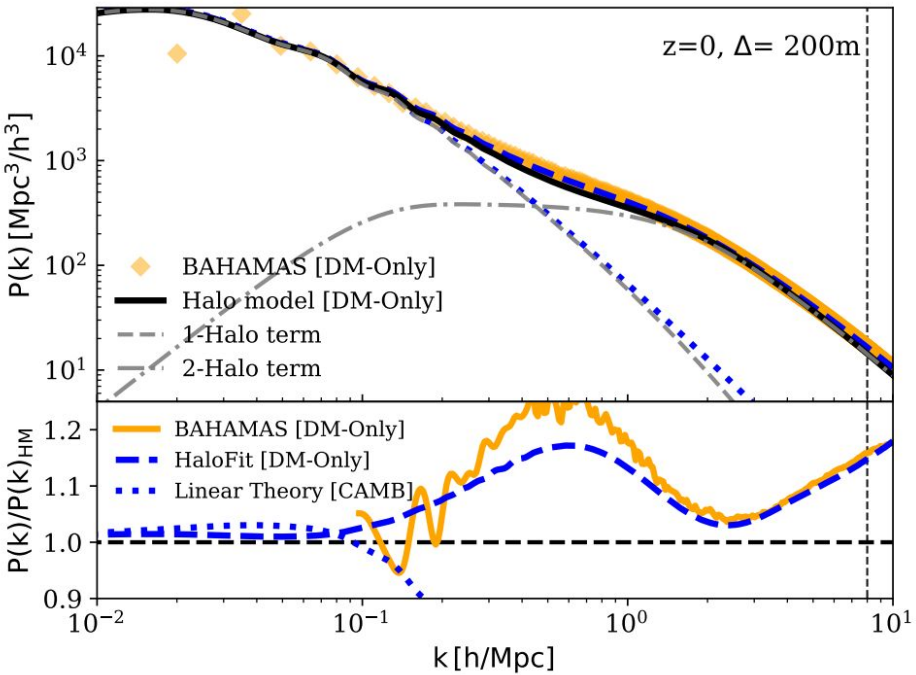

# BIASED TRACERS OF THE DENSITY FIELD

# HALO BIAS

**Halo formation is not a random process; haloes are not a Poisson sampling of the matter field. Rather, they only form where the (smoothed) density field has a sufficiently high value: the critical overdensity for collapse. This `threshold' causes haloes to be biased tracers of the mass distribution: Because of the modulation of the small-scale density field by the long-wavelength modes, overdense regions (on large scales) contain enhanced abundance of dark matter haloes, so that these haloes display enhanced clustering.**

Example notebook

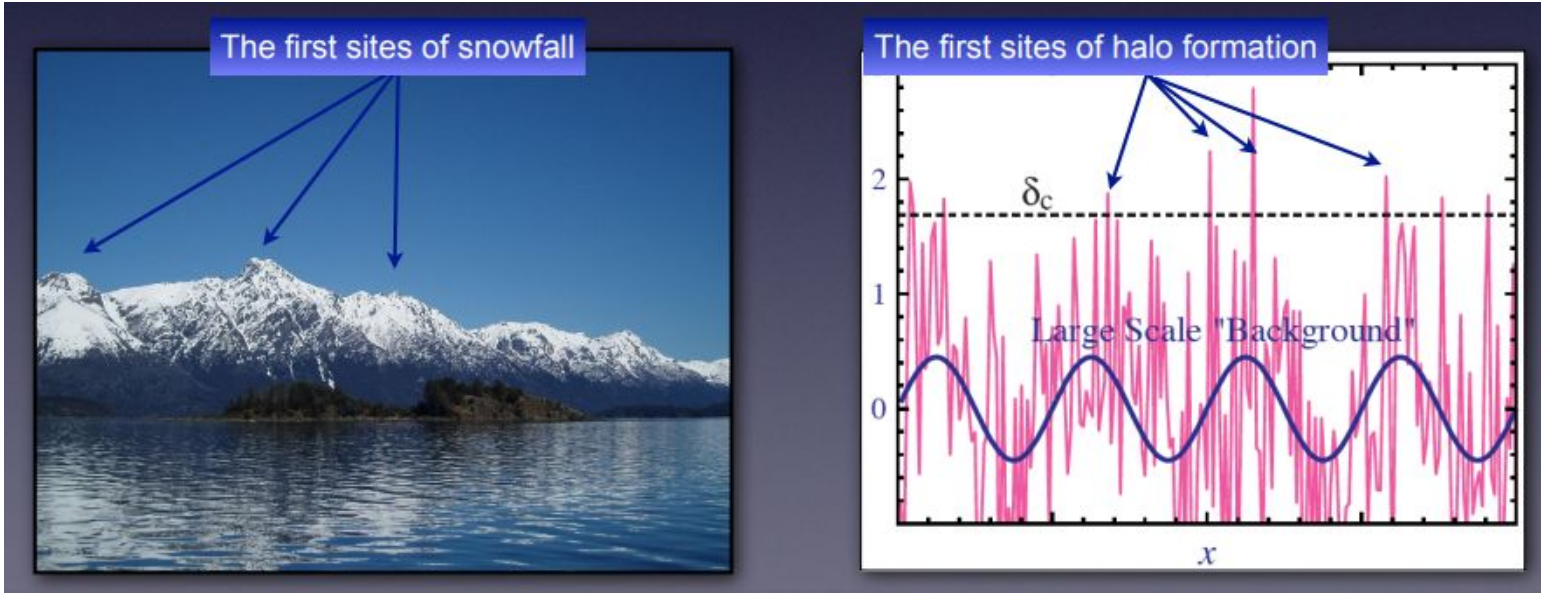

# 2PT CORRELATION FUNCTION: BIAS

**The collapsed structures we observe today, that is, galaxies and galaxy clusters, are formed at the locations peaks of the matter density field and more massive objects correspond to higher peaks. Thus, we expect their distribution to be a biased tracers of the underlying mass distribution and the bias grows with the mass of the objects.**

$$\delta_h = b_h \delta_m$$

$$\xi_{hh}(r) = \langle \delta_h(x)\delta_h(x+r)\rangle = b_h^2 \xi_{mm}$$

$$\mathcal{F} \downarrow\uparrow \mathcal{F}^{-1}$$

$$P_{hh}(k) = \langle \tilde{\delta}_h(k)\tilde{\delta}_h^{\,*}(k')\rangle = b_h^2 P_{mm}(k)$$

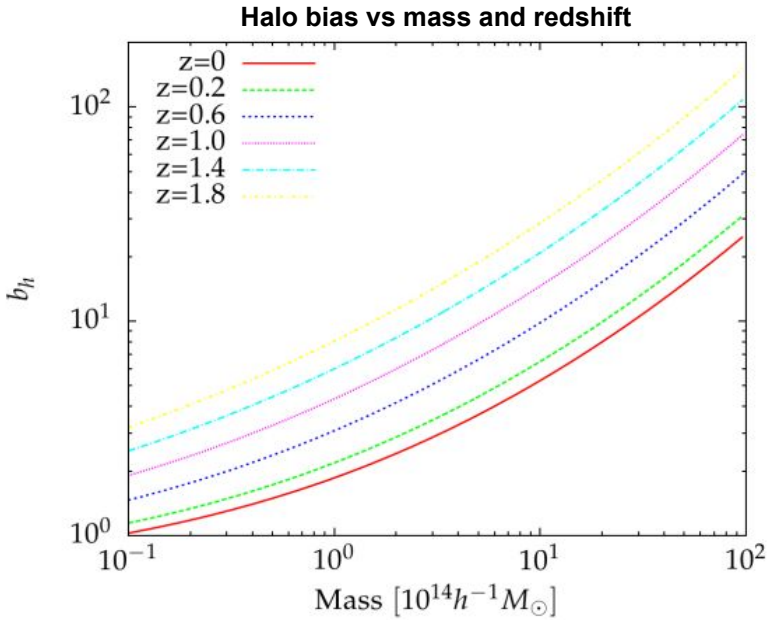

# TRACERS OF THE MATTER DENSITY FIELD

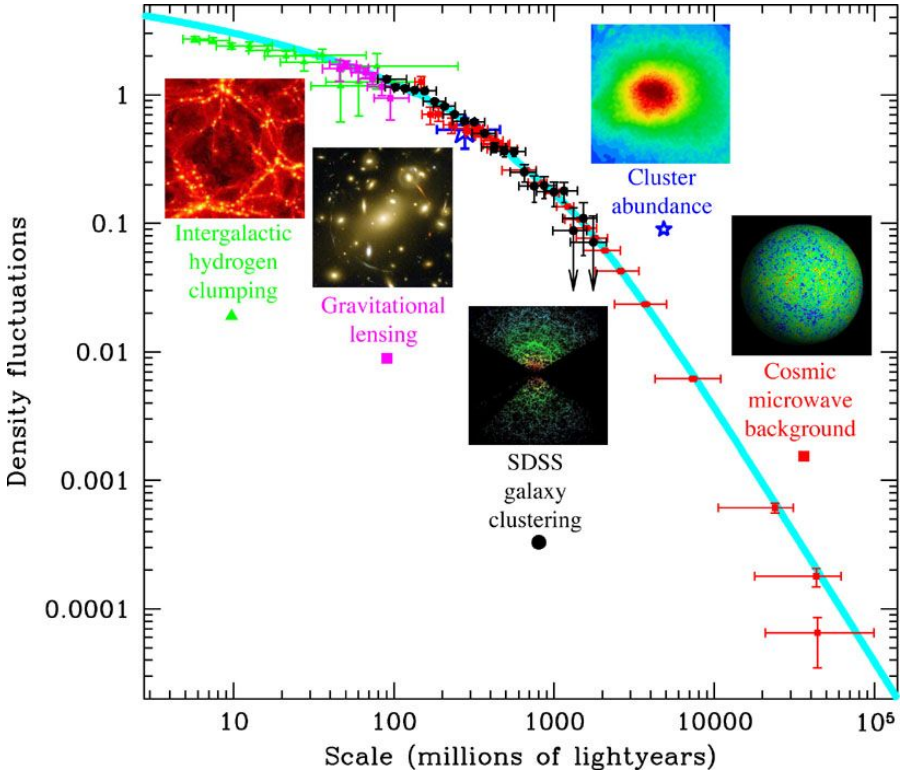


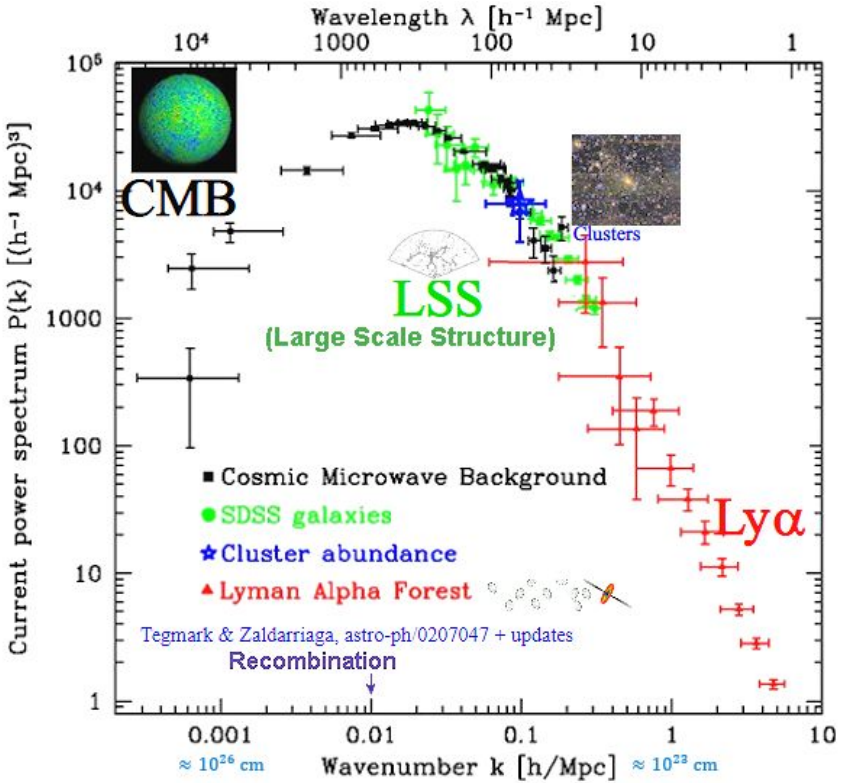

# TRACERS OF THE MATTER DENSITY FIELD

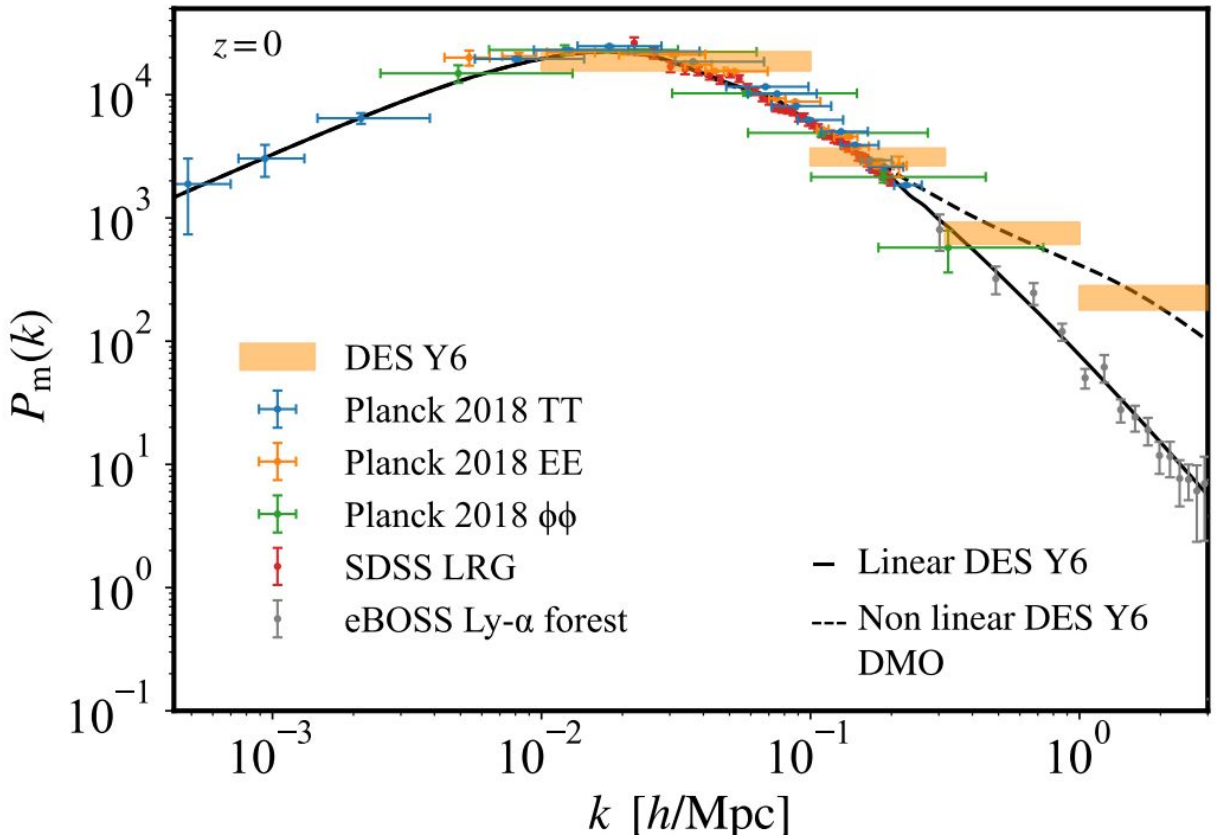


https://arxiv.org/pdf/2602.10065

# CLUSTERING OF CLUSTERS

**Galaxy clusters, arising from the highest density peak of the matter density field, have the largest bias.**
**Their bias can be predicted from theory (or calibrated from simulations) from the halo mass function:**

$$\delta^{\mathrm{L}}_{\mathrm{halo}} = \frac{\mathcal{N}(M|\delta_0, S_0)}{(\mathrm{d}n(M)/\mathrm{d}M)V_0} - 1$$

**On the other hand, forming on the rare high density peaks of the matter density field, galaxy clusters are a sparse tracer of $\delta_m$, and their 2pt CF signal is largely disturbed by shot noise.**

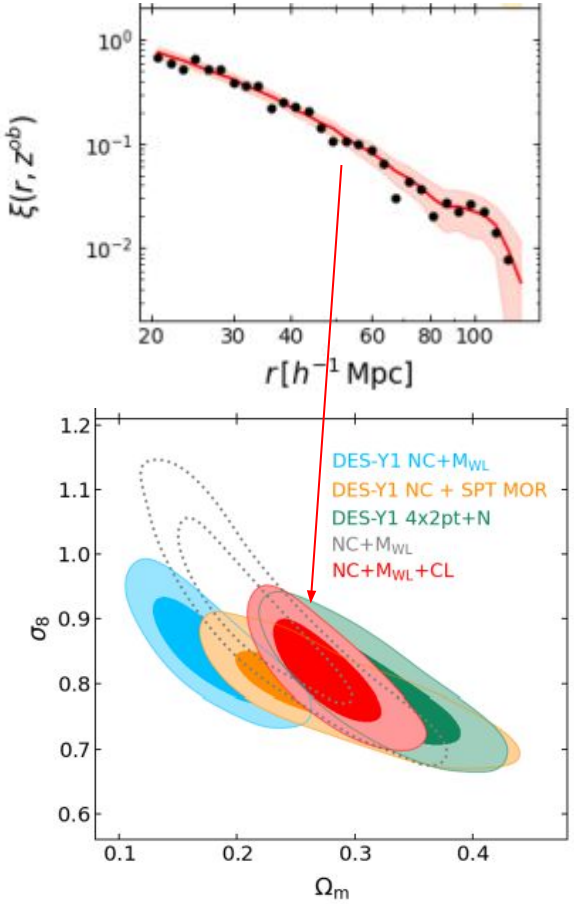


https://arxiv.org/pdf/2310.09146.pdf

# CLUSTERING OF GALAXIES

**Galaxies provide a much wider sample (~$10^8$) compared to clusters (~$10^{3\text{-}4}$), thus greatly reducing the shot noise on 2pt CF measurements. On the other hand galaxy bias cannot be predicted from theory, and in general it depends on the specific galaxy sample (e.g. color and/or magnitude selection) employed for the analysis.**

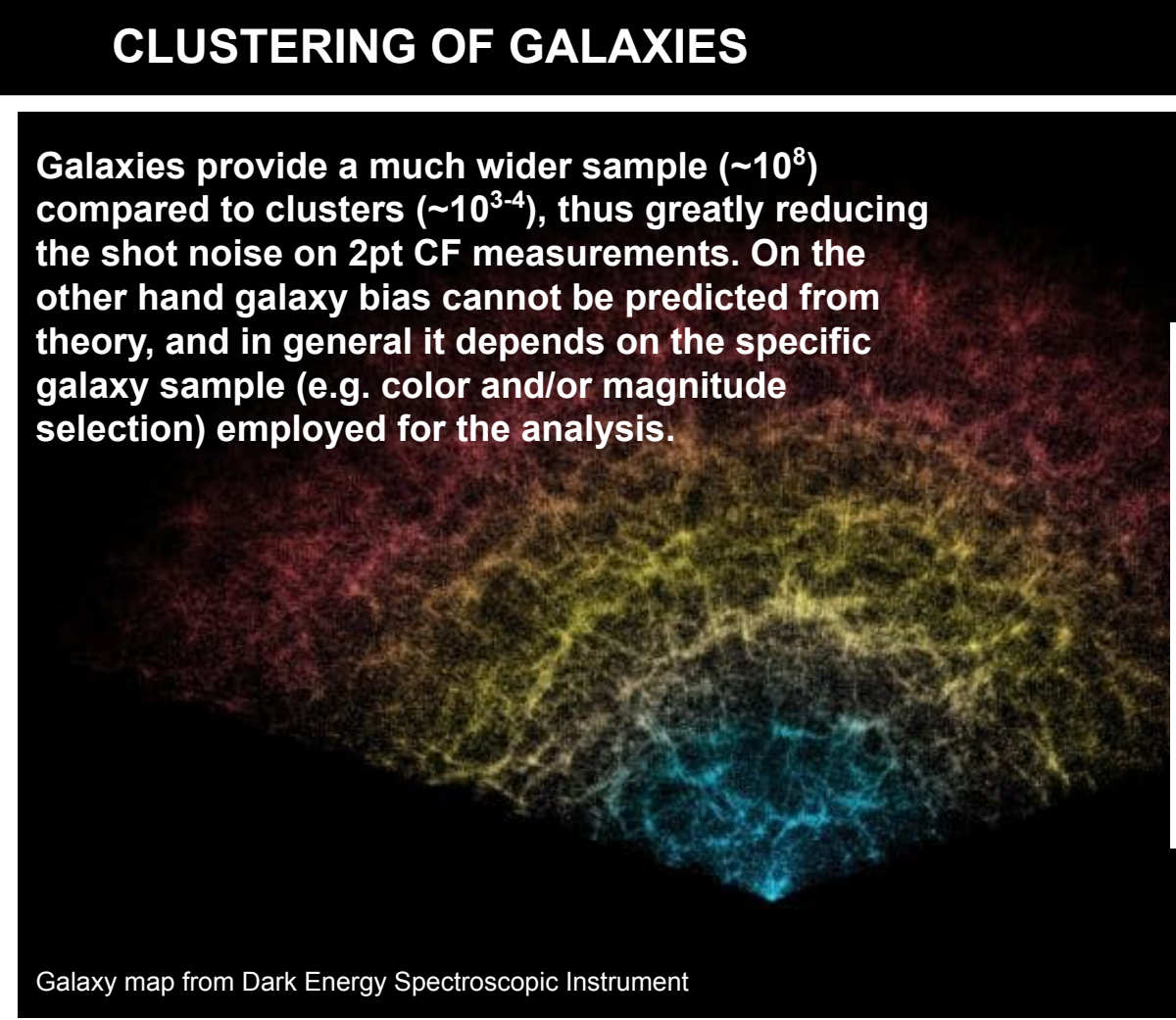

Galaxy map from Dark Energy Spectroscopic Instrument

**The correlation function of the CMASS galaxies in the [0.538 − 0.592] redshift range.**

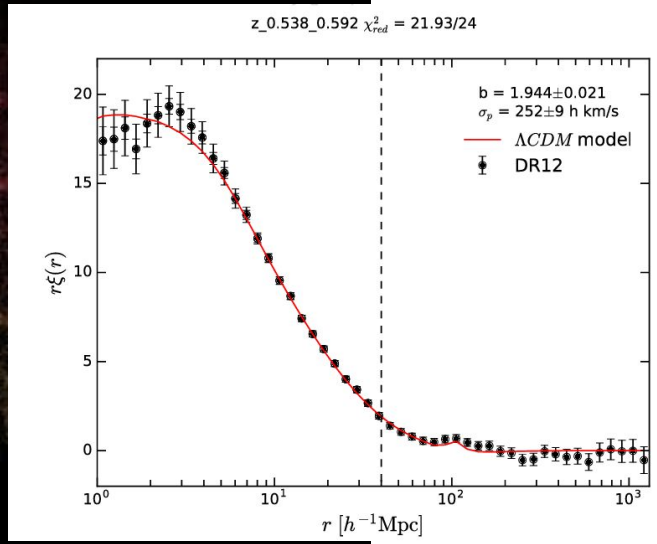

# SPECTROSCOPIC VS PHOTOMETRIC SURVEYS

**The clustering signal is 3D. However, while angular positions are in general easy to measure, the radial distance can be inferred only from redshift measurements.**

**Depending on the data we can measure:**

**1) Spectroscopic redshift [$\sigma_z \sim 0.001\times(1+z)$] : Measuring the spectrum of galaxies, and hence the shift of known emission/absorption lines.**

**2) Photometric redshift [$\sigma_z \sim 0.01\times(1+z)$]: Estimate from broadband photometry by fitting template spectra predicted from galaxy Spectral Energy Distribution or from observed galaxies with known spectroscopic redshift.**

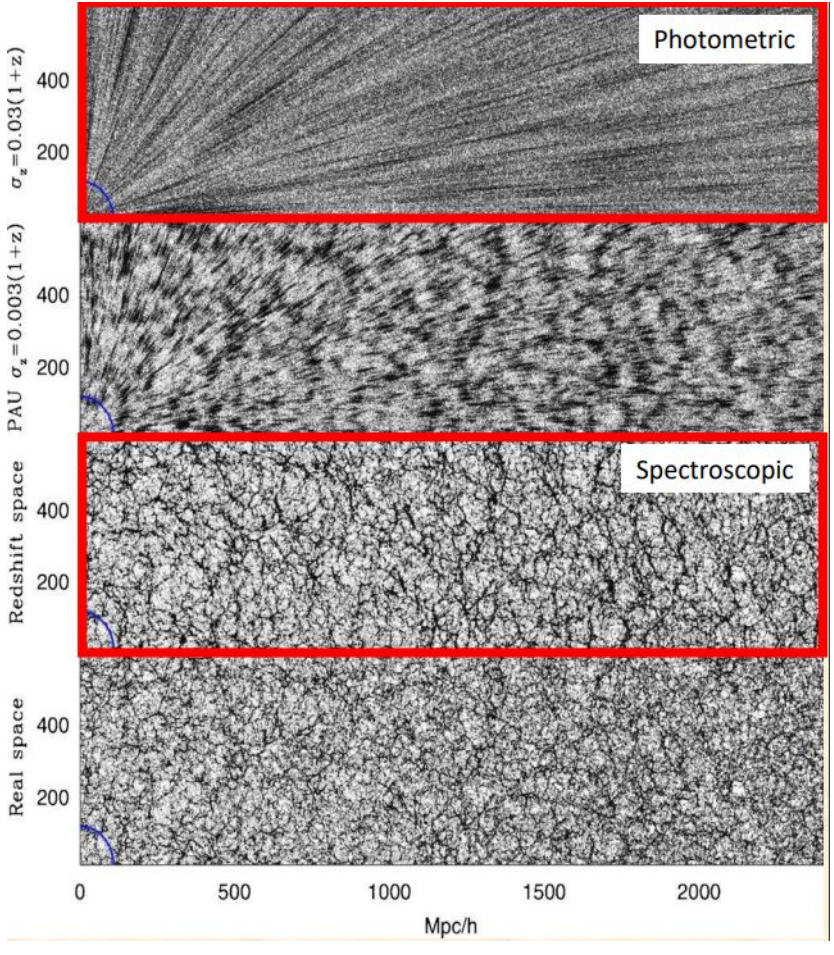

# SPECTROSCOPIC VS PHOTOMETRIC SURVEYS

Photometric redshifts can be measured much faster than their spectroscopic counterparts. In spectroscopy, the light from the galaxy is separated into narrow wavelength bins a few angstroms across. Each bin then receives only a small fraction of the total light from the galaxy. Hence, to achieve a sufficiently high signal-to-noise ratio in each bin, long integration times are required, and only luminous sources can be targeted. For photometry, however, the bins are much larger, and it requires only a short exposure time to reach the same signal-to-noise ratio. Further, imaging detectors usually cover a greater area of the sky than multi-object spectrographs. This means that the redshifts of more objects can be measured simultaneously by using photometry than by spectroscopy. Thus in general:

**Spectroscopic survey:**

- Accurate 3D reconstruction
- Medium depth
- Low density
- Strong selection effects

**Photometric survey:**

- Low resolution along the line-of-sight
- Usually deeper and larger area (i.e. larger volume)
- High density
- ~ No selection effects

# SPECTROSCOPIC VS PHOTOMETRIC SURVEYS

**Redshift errors perturbs the distance measurements along the line of sight affecting the clustering signal by reducing 2pt CF slope and smearing the BAO feature (see later)**

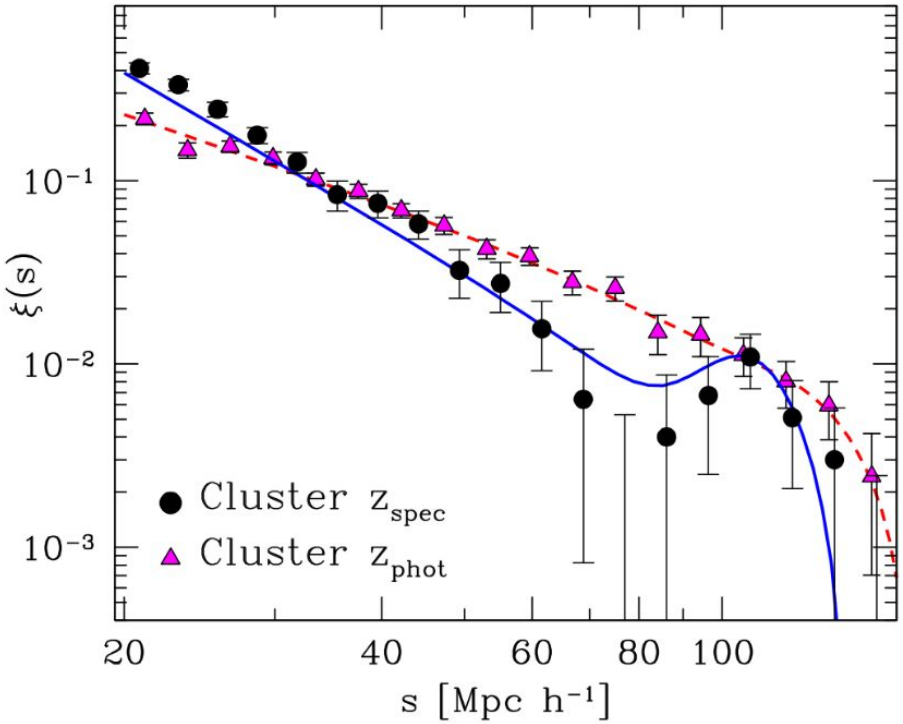


**Figure 3.5:** Comparison between the redshift-space two-point correlation functions of spectroscopic (black dots) and photometric (magenta triangles) cluster samples, selected from the Sloan Digital Sky Survey, with measured redshifts in the range $0.1 < z < 0.42$. The lines show the best-fitting empirical models obtained for spectroscopic (blue lines) and photometric clusters (dashed red lines). Credits to Veropalumbo et al. (2014).

# ANGULAR 2PT CORRELATION FUNCTION

**If the resolution along the line of sight is poor (e.g. in a photometric survey) or none (CMB last scattering surface), one can measure the angular correlation function. In analogy with $\xi(r)$, we can define $w(\vartheta)$ as the excess probability of finding two tracers separated by an angular distance $\vartheta$ on the sky:**

$$dP(\theta) = n(1 + w(\theta))d\Omega$$

**$w(\vartheta)$ is related to the real space correlation function via a line-of-sight projection.**

$$w(\theta) = \langle \delta(\hat{n})\delta(\hat{n} + \hat{\theta}) \rangle =$$

$$= \int \int dz_1 dz_2 \xi(\sqrt{r^2(z_1) + r^2(z_2) - 2r(z_1)r(z_2)cos\theta})$$

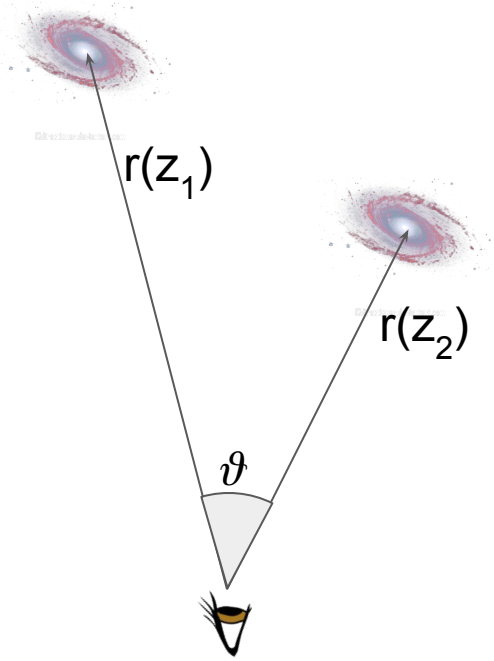

# ANGULAR 2PT CF AND POWER SPECTRUM

**Similarly to the real space 2pt CF we can relate the angular CF to the angular power spectrum, $C_\ell$, via the multipole expansion:**

$$w(\theta) = \sum_\ell \left( \frac{2\ell + 1}{4\pi} \right) L_\ell(\cos\theta) C_\ell$$

Legendre polynomial of degree $\ell$

$$C_\ell = 2\pi n_\Omega \int_{-1}^{+1} w(\theta) L_\ell(\cos\theta) \mathrm{d}\cos\theta$$

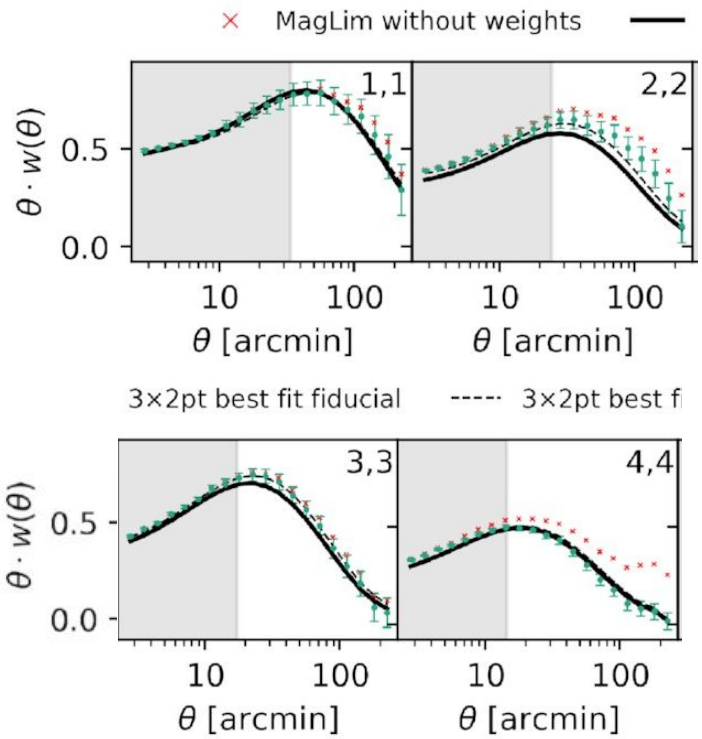


DES Y3 angular galaxy clustering in 4 tomographic bins between 0.2<z<0.85

# SPECTROSCOPIC VS PHOTOMETRIC SURVEYS

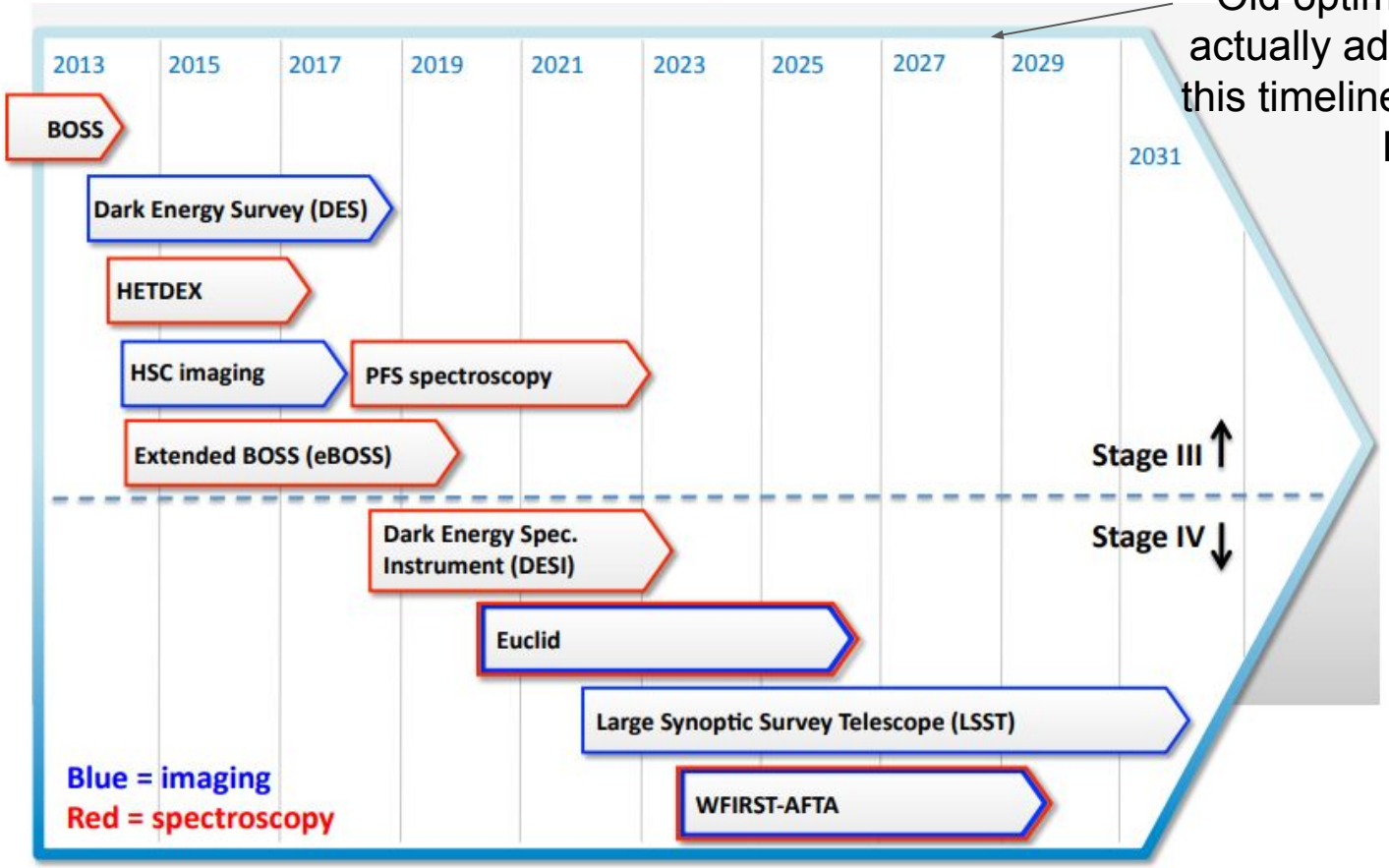


Old optimistic slide, actually add ~4 yr on this timeline for stage IV surveys

# SPECTROSCOPIC VS PHOTOMETRIC SURVEYS

## Galaxy surveys

| Project | Dates | Area/deg2 | Data | Redshift | Methods |
|---|---|---|---|---|---|
| BOSS | 2008-2014 | 10000 | Opt-S | 0.3-0.7 (gal)<br>2-3.5 (Lyα Forest) | BAO/RSD |
| DES | 2013-2018 | 5000 | Opt-I | 0.2-1.5 | WL/CL/BAO/SN |
| eBOSS | 2014-2020 | 7500 | Opt-S | 0.6-2.0 (gal/QSO)<br>2-3.5 (Lyα Forest) | BAO/RSD |
| SuMIRE | 2014-2024 | 1500 | Opt-I<br>Opt-NIR-S | 0.2-1.5<br>0.8-2.4 (gals) | WL/CL/<br>BAO/RSD |
| HETDEX | 2014-2019 | 300 | Opt-S | 1.9-3.5 (gals) | BAO/RSD |
| DESI | 2019-2024 | 14000 | Opt-S | 0-2 (gals)<br>2-3.5 (QSO/Lyα Forest) | BAO/RSD |
| LSST | 2020-2030 | 20000 | Opt-I | 0.2-2 | WL/CL/BAO/SN |
| Euclid | 2020-2026 | 15000 | Opt-I<br>NIR-S | 0.2-2<br>0.7-2.2 (gals) | WL/CL/BAO/RSD |
| WFIRST | 2024-2030 | 2200 | NIR-I<br>NIR-S | 1.0-3.0 (gals) | WL/CL/SN/BAO/RSD<br>From PDG 2016 |

# BARYONIC ACOUSTIC OSCILLATIONS

The clustering of matter encodes a preferred scale, the *sound horizon at the baryon drag epoch* of the early universe. This feature, which is imprinted on the matter distribution of the early universe by physics around recombination and earlier, is stretched with the expansion of the universe, appearing at a comoving galaxy separation of $r_d$ ~ 150 Mpc. Since galaxies trace the matter content of the universe, the BAO feature is transferred into galaxy clustering, where it manifests as a single localised peak in the galaxy correlation function and an oscillatory signature, or “wiggles”, in the galaxy power spectrum. The signature is also visible in other tracers of mass such as fluctuations in the Lyman-α forest — spectral features that indicate the radial distribution of neutral hydrogen clouds between the observer and distant quasars, as well as the CMB. Using BAO we can study the evolution of the Universe’s geometry, thus test for dark energy dynamics and spatial curvature, and in combination with other probes constrain the Hubble constant, the sum of neutrino masses, and the number of light species.

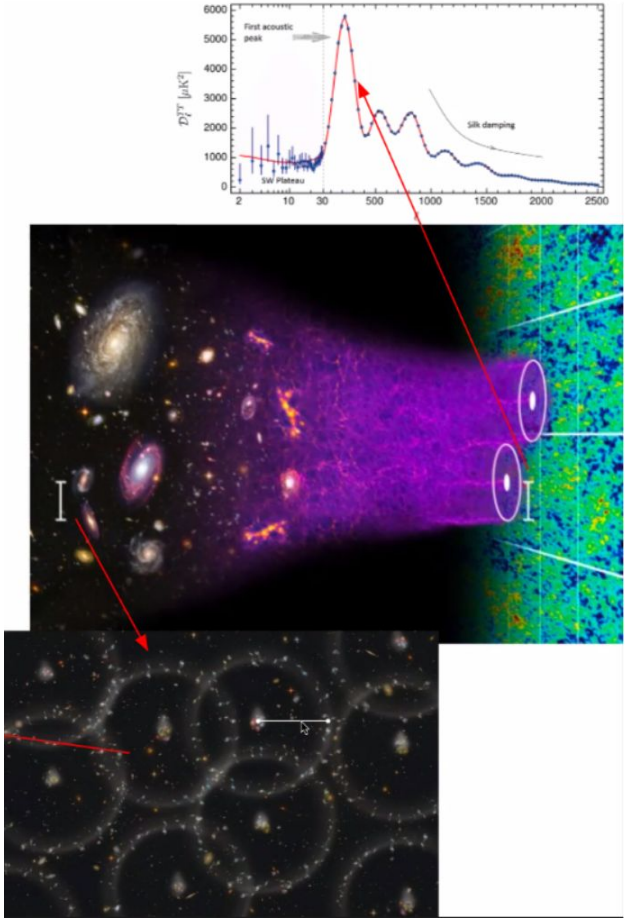

# BARYONIC ACOUSTIC OSCILLATIONS

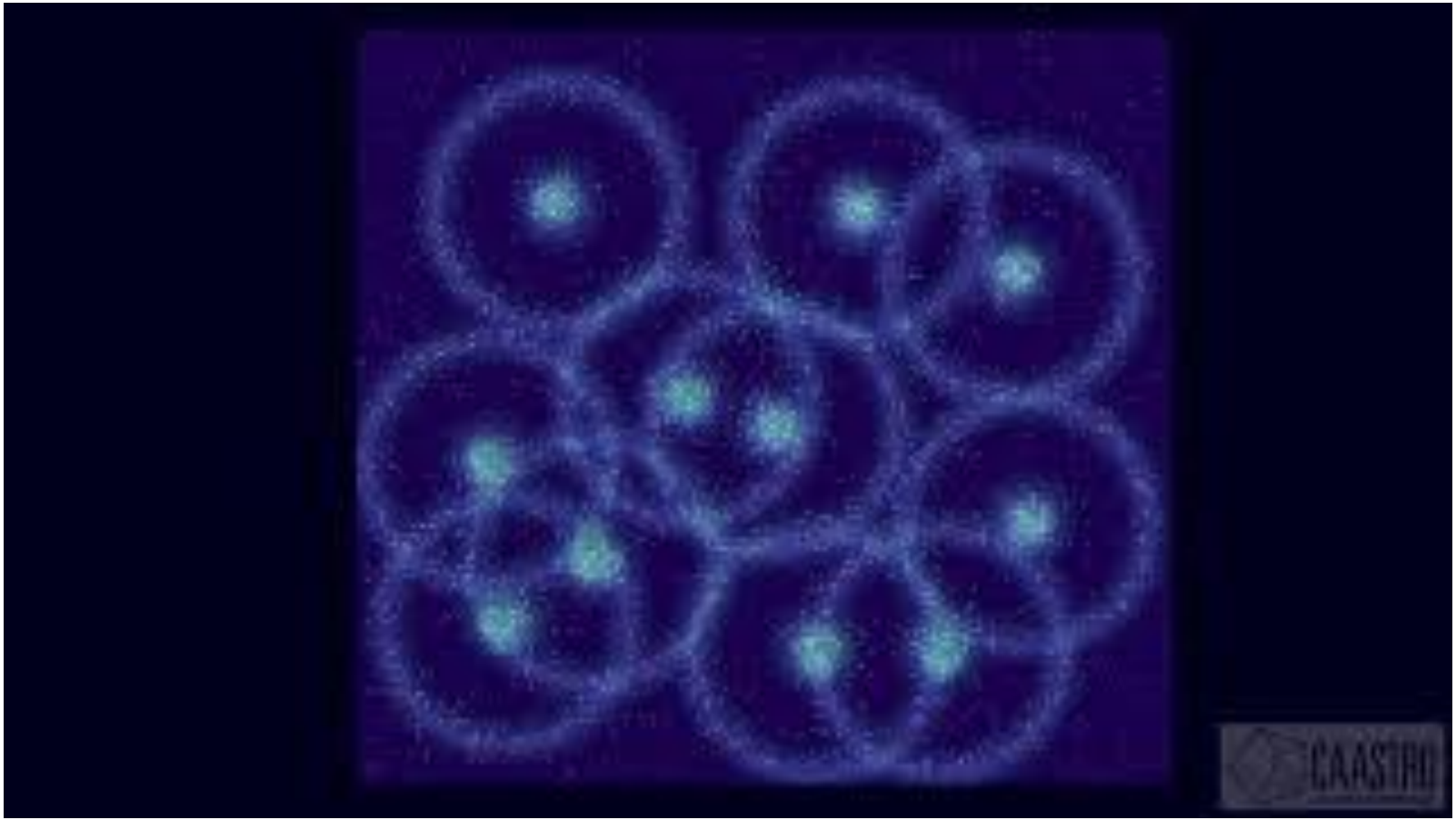

# BAO AS STANDARD RULER

**The physics of the propagation of the baryon waves in the early universe is fairly simple, and the sound horizon at drag epoch (~recombination) can be predicted, making $r_d$ a standard ruler. The (comoving) distance that sound can travel before the drag epoch (which indicates the time when the baryons decoupled at $z_d \approx 1060 \approx z_*$ ) is given by:**

Speed of sound

$$r_{\rm d} = \int_{z_{\rm d}}^{\infty} \frac{c_{\rm s}(z)}{H(z)} dz \qquad c_{\rm s}(z) = \frac{c}{\sqrt{3\left(1+\frac{3\rho_{\rm B}(z)}{4\rho_{\gamma}(z)}\right)}}$$

$$r_{\rm d} = \frac{147.05}{\rm Mpc}\left(\frac{\omega_{\rm m}}{0.1432}\right)^{-0.23}\left(\frac{N_{\rm eff}}{3.04}\right)^{-0.1}\left(\frac{\omega_{\rm b}}{0.02236}\right)^{-0.13}$$

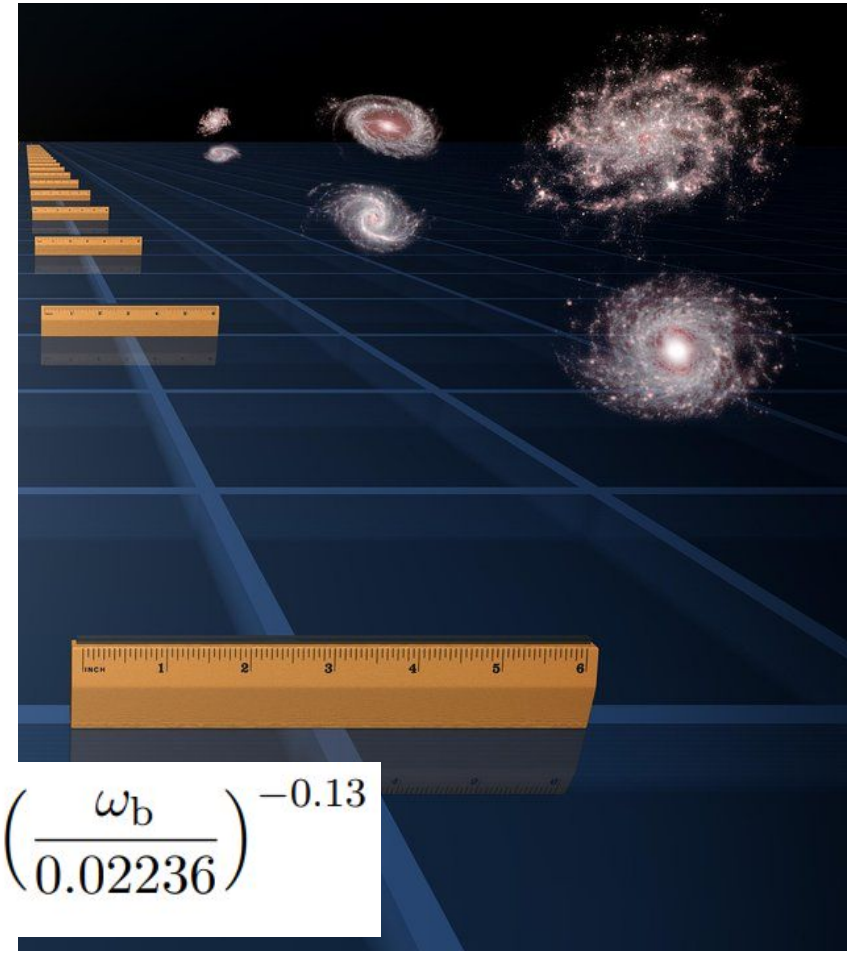

# BARYONIC ACOUSTIC OSCILLATIONS

- **Perpendicular to the observer's line-of-sight, a preferred angular separation of galaxies θ can be observed:**

$$\theta = \frac{r_d(z)}{(1+z)d_A(z)}$$

- **Parallel to the observer's line-of-sight, a preferred redshift separation Δz can be observed:**

$$\Delta z = \frac{H(z)r_d}{c}$$

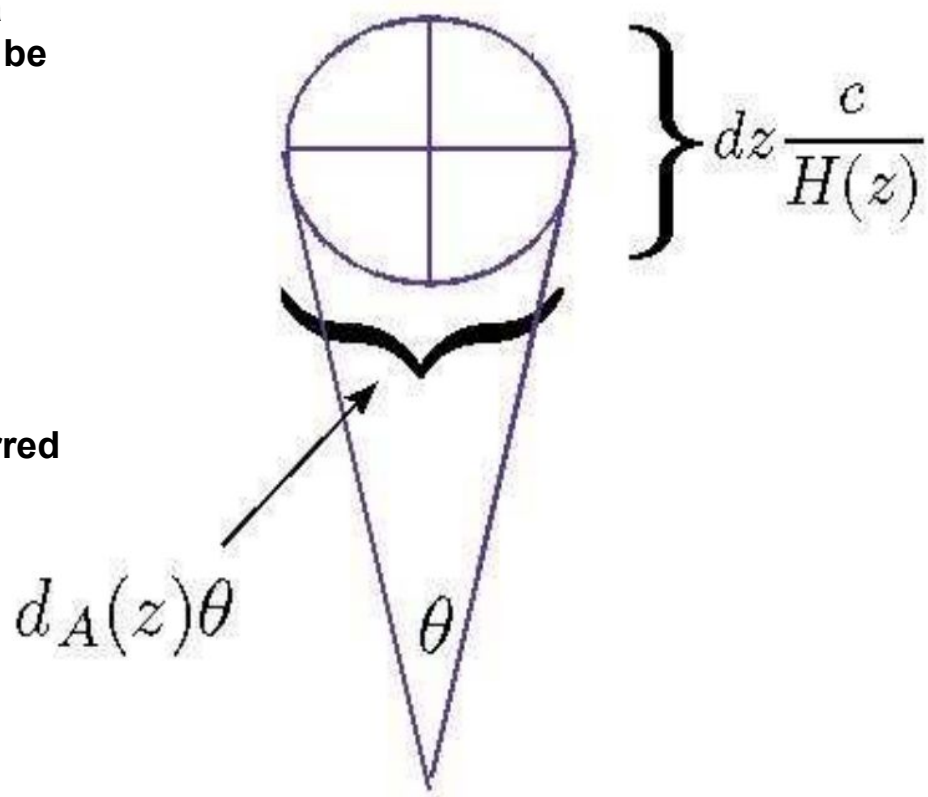

# BARYONIC ACOUSTIC OSCILLATIONS

- **For a flat LCDM universe, at late time ($z \ll z_{eq}$):**

**Angular diameter distance:**

$$d_{\mathrm{A}}(z) = \frac{c}{H_0} \frac{1}{(1+z)} \int_0^z \frac{dz}{\left[\Omega_{\mathrm{m},0}\,(1+z)^3 + \Omega_{\Lambda,0}\right]^{1/2}}$$

**Hubble parameter:**

$$H(z) = H_0 \sqrt{\Omega_{m,0}(1+z)^3 + \Omega_{\Lambda,0}}$$

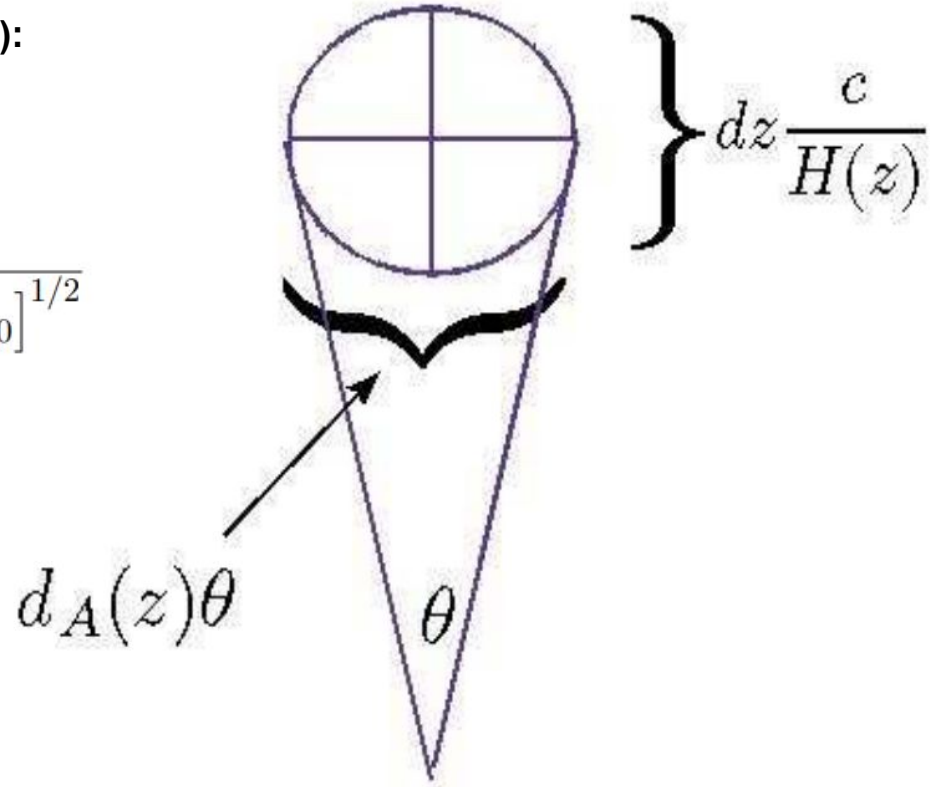

# ANGULAR DIAMETER DISTANCE

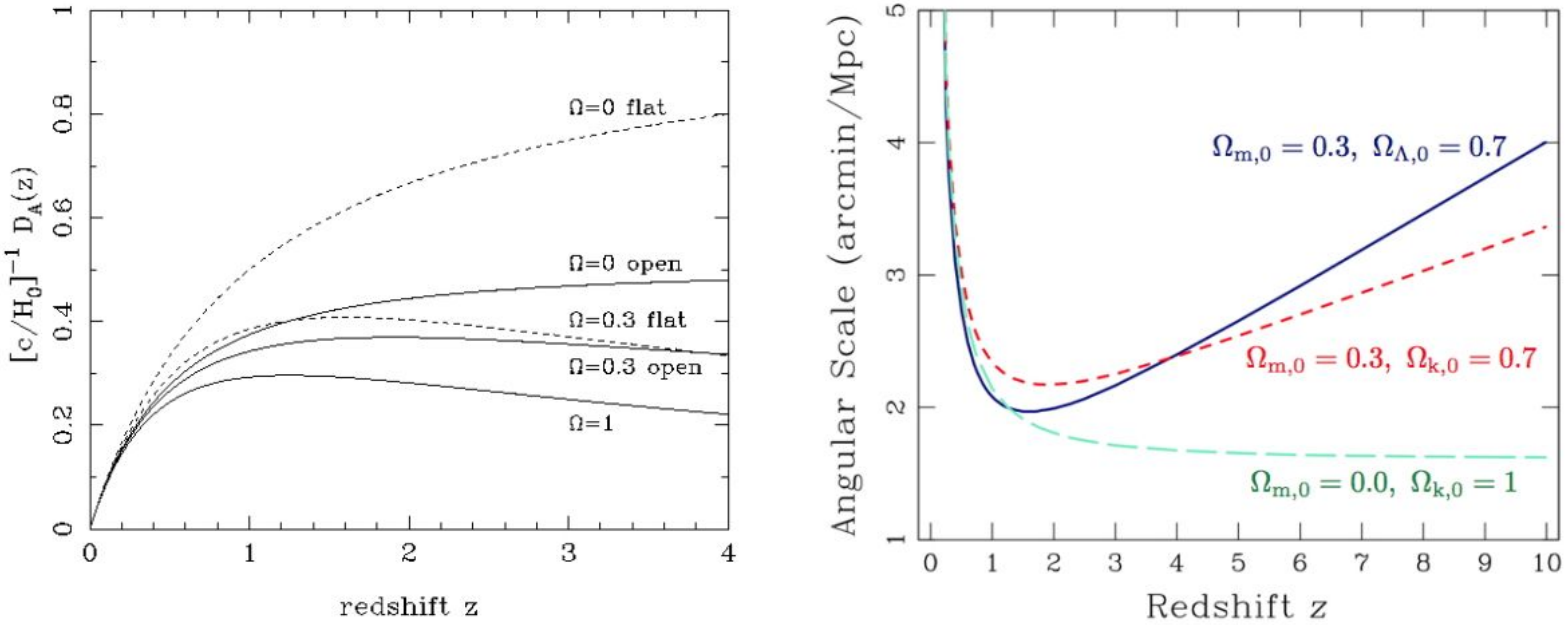


Figure 5.4: *Left:* Plot of the angular diameter distance, $d_{\rm A}$, (in units of $c/H_0$) as a function of redshift $z$ in different cosmologies (in this figure $\Omega \equiv \Omega_{\rm m,0}$). *Right:* Angle subtended on the sky by an object of proper size $D = 1\,{\rm Mpc}$ as a function of redshift for three different cosmologies, as indicated.

# ANGULAR DIAMETER DISTANCE

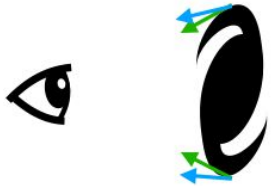

**The turnover point occurs because of the expansion of the universe and the finite speed of light: very distant objects were closer to us when they emitted the light we see today. At that time they spanned a larger angle.**

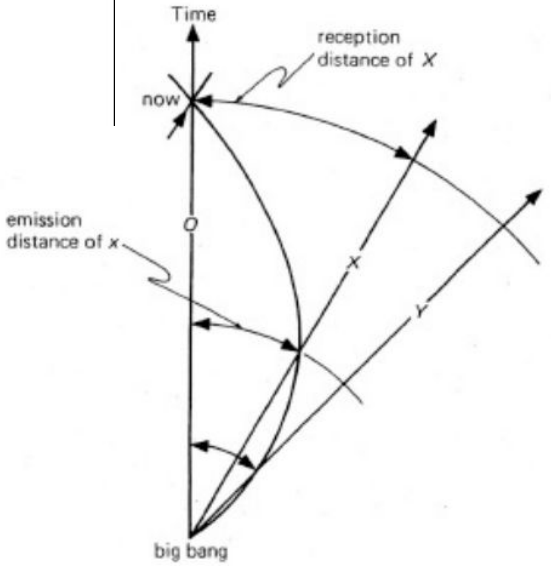


Figure 5.9: O's lightcone curves back into the Big Bang. The diagram shows the reception and emission distances of galaxies $X$ and $Y$. Although galaxy $Y$ has a greater reception distance, its emission distance is smaller than that of $X$. Thus $Y$, which is now further away than $X$, was closer to us than $X$ at the time of the emission of the light which we now see (reproduced from E. R. Harrison's *Cosmology*).

# BAO SCALE FROM GALAXY SURVEY

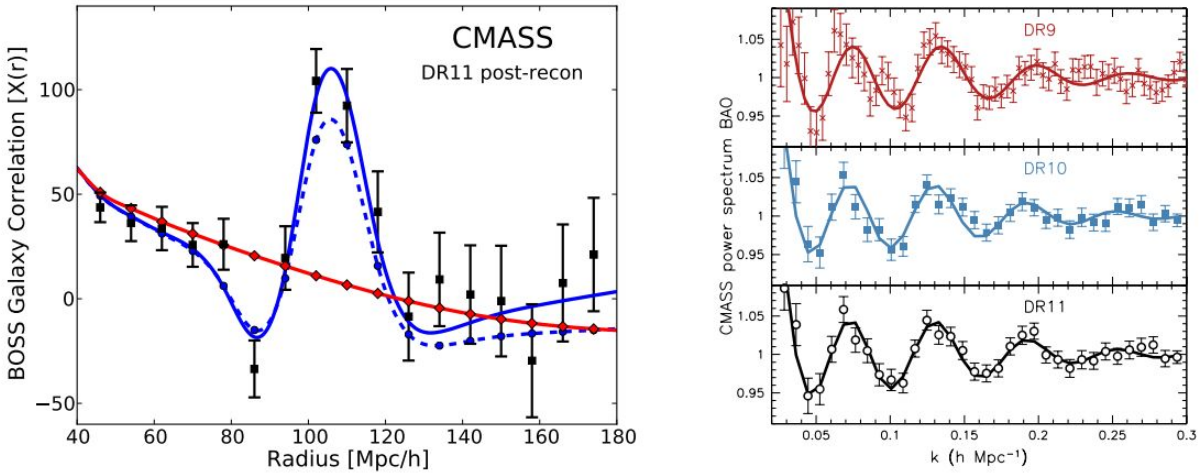


Figure 14.8: *Left:* Baryonic acoustic peak in the two-point correlation function of $\sim 10^6$ galaxies at redshifts $0.4 < z < 0.7$ as determined by the Baryon Oscillation Spectroscopic Survey (BOSS) project. The blue solid line is the best-fit BAO model, while the red line shows the fit by a model which does not include the BAO. *Right:* The BAO feature of the left panel is shown here in the power spectrum of the galaxy distribution: a spike in real space becomes a series of ripples in $k$-space. The results for three successive data releases of the BOSS project are shown separately. The data and the best fits have been normalised by dividing by the smooth model shown by the red continuous line in the left panel. (Figures reproduced from Anderson et al. 2014).

# BAO SCALE FROM GALAXY SURVEY

The inset for each color-coded section of the map includes an image of a typical galaxy or quasar from that section, and also the signal of the pattern that the eBOSS team measures there. As we look out in distance, we look back in time. So, the location of these signals reveals the expansion rate of the Universe at different times in cosmic history.

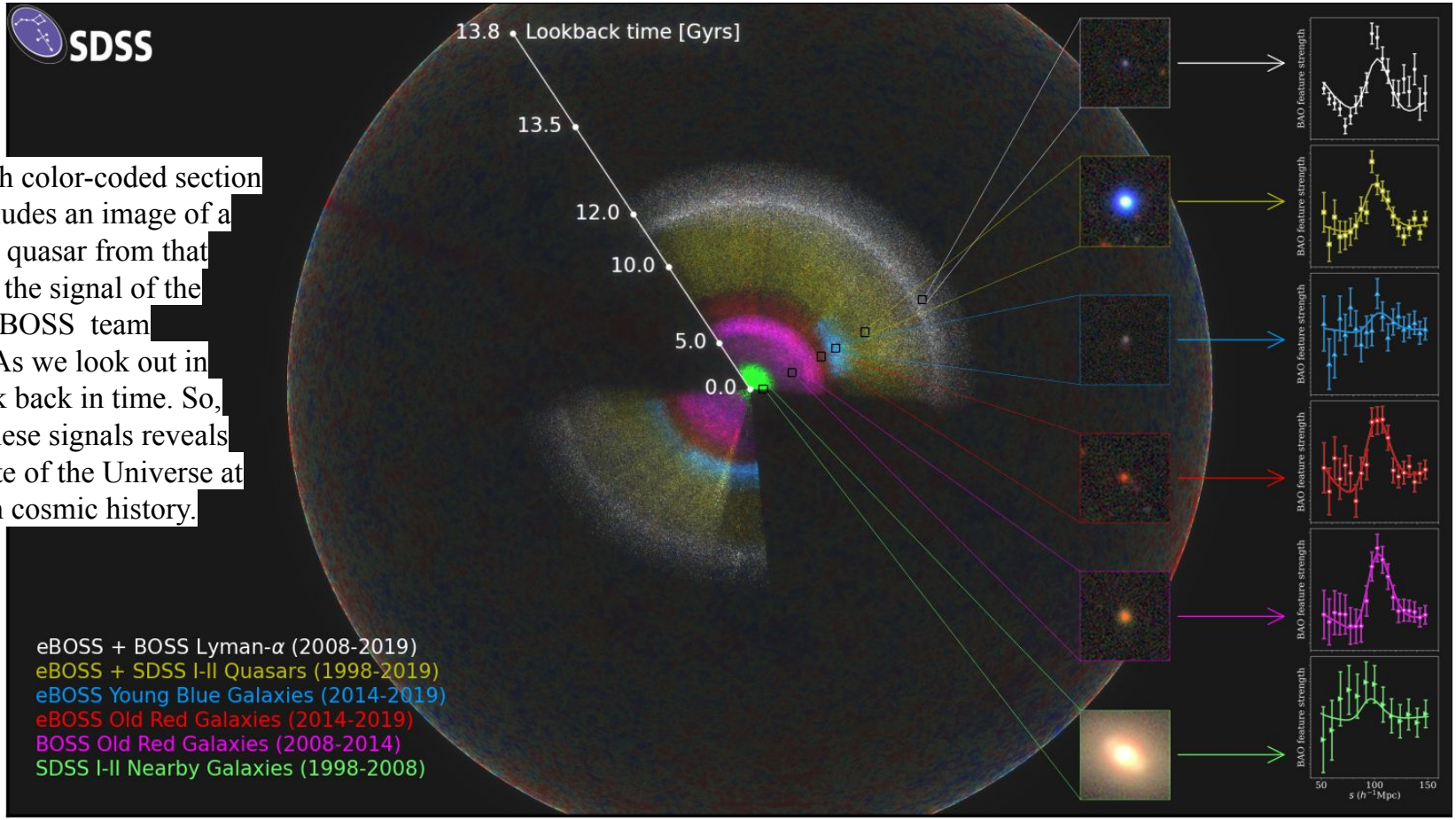

# BAO SCALE FROM GALAXY SURVEY

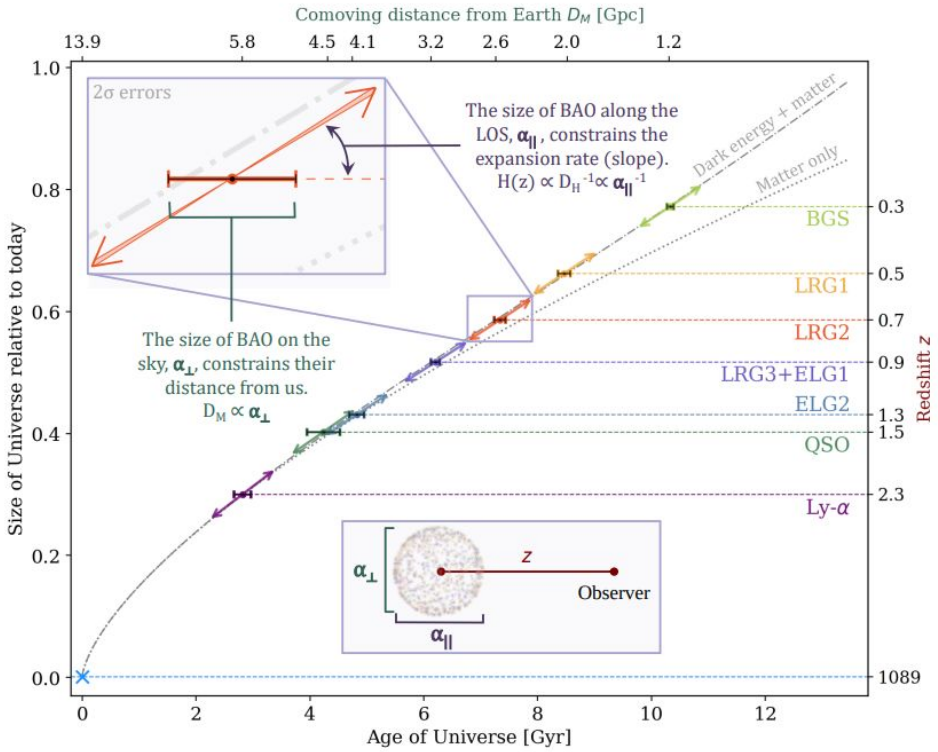


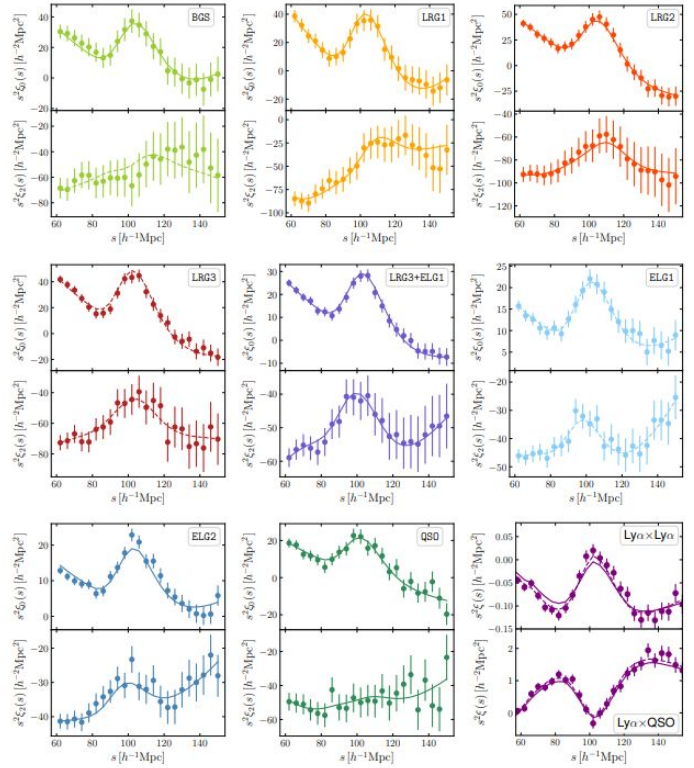


FIG. 5. The first eight panels show the multipole moments of the DESI DR2 correlation functions of galaxies and quasars, where the upper and lower subpanels display the monopole and quadrupole moments, respectively. The filled circles correspond to the data measurements and the lines show the best-fit BAO model. We use a solid line for model fits to those samples used in our analysis, and a dashed line otherwise. Error bars represent 68% confidence intervals. The last panel (bottom right) shows the autocorrelation of the Lyα forest (upper sub-panel), and the cross-correlation between the Lyα forest and the quasars (bottom sub-panel), where the 2D clustering information has been compressed into a single wedge. The solid line in this panel is the baseline model, while the dashed line includes a broad-band polynomial variation that provides a slightly better fit, but does not significantly shift the BAO position (see [61] for details).

https://arxiv.org/pdf/2503.14738

# BAO AS STANDARD RULER

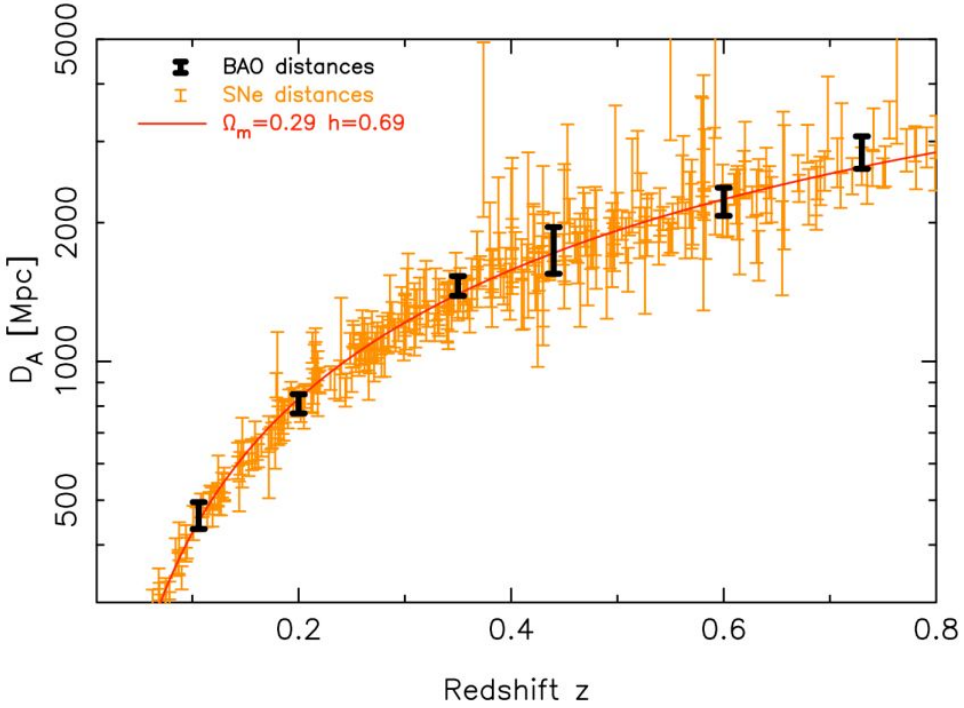


Figure 14.12: Comparison between the SN and BAO mapping of the cosmic distance scale. For the purpose of this figure, the SN $d_{\rm L}$ measurements have been converted to $d_{\rm A}$, assuming $d_{\rm A}(z) = d_{\rm L}(z)/\left(1+z\right)^2$ (Figure reproduced from Blake et al. 2011).

# REDSHIFT SPACE DISTORTIONS

**Due to peculiar velocities (along the line of sight), the redshift distances available from a galaxy redshift survey deviate from the true, proper distances. This results in redshift space distortions in the clustering measurements.**

$$v = v_{\rm exp} + v_{\rm pec} = H_0 d(z) + v_{\rm pec}$$

$$z_{\rm obs} = z_{\rm exp} + \frac{v_{\rm pec}}{c}(1 + z_{\rm exp})$$

**L.o.s. Proper Distance measured in redshift space:**

$$s = \frac{v}{H_0} = d(z) + \frac{v_{\rm pec}}{H_0}$$

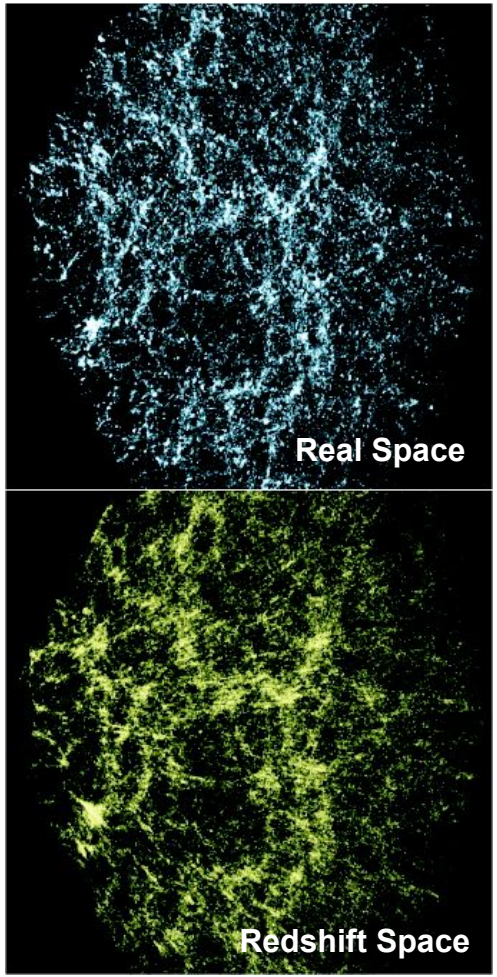

# REDSHIFT SPACE DISTORTIONS

- **Kaiser effect:**

**On large scales, peculiar velocities reflect the (linear) infall motions towards overdensities, causing a circle in real space to appear "squashed" in redshift space.**

- **Finger-of-God effect:**

**On small scales, peculiar velocities are due to the nonlinear virialized motion of galaxies inside their host haloes, causing a circle in real space to appear "stretched" in redshift space.**

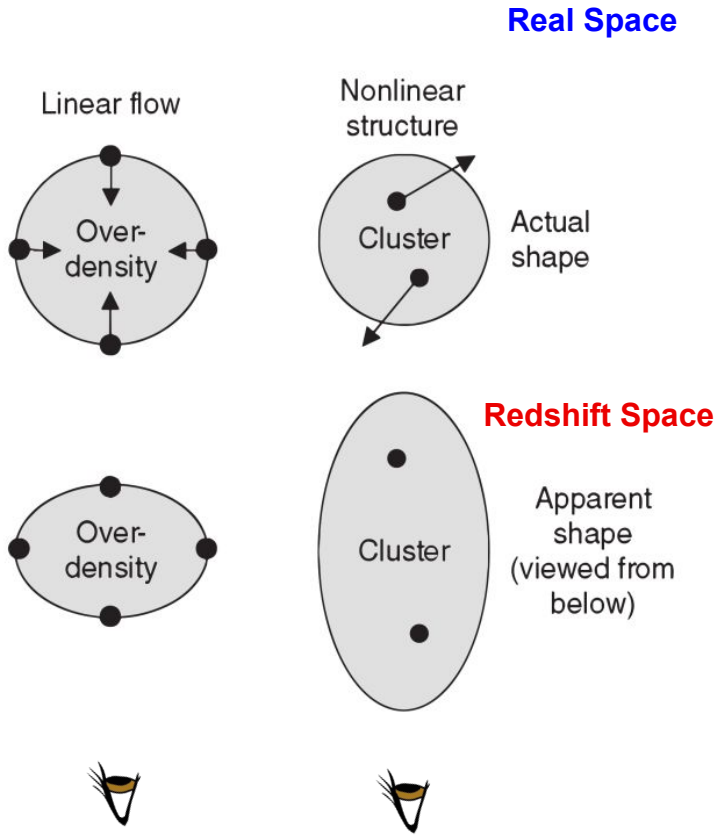

# REDSHIFT SPACE DISTORTIONS

Only radial distances are modified by the Doppler effects of peculiar velocities. The complication is that the peculiar velocities arise from the clustering itself. Thus, the apparent clustering pattern in redshift space differs systematically from that in real space and the spatial correlation function of galaxies, which is isotropic in real space is no longer isotropic in redshift space.

We can decompose the distance between two galaxies in their perpendicular and parallel component along the l.o.s.:

$$\pi \equiv \frac{|s \cdot l|}{|l|} \qquad \sigma \equiv \sqrt{s \cdot s - \pi^2}$$

And compute $\xi(\pi, \sigma)$

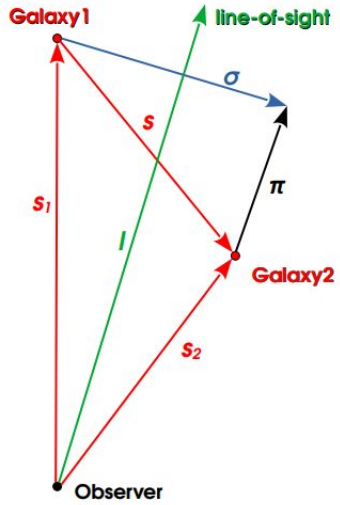


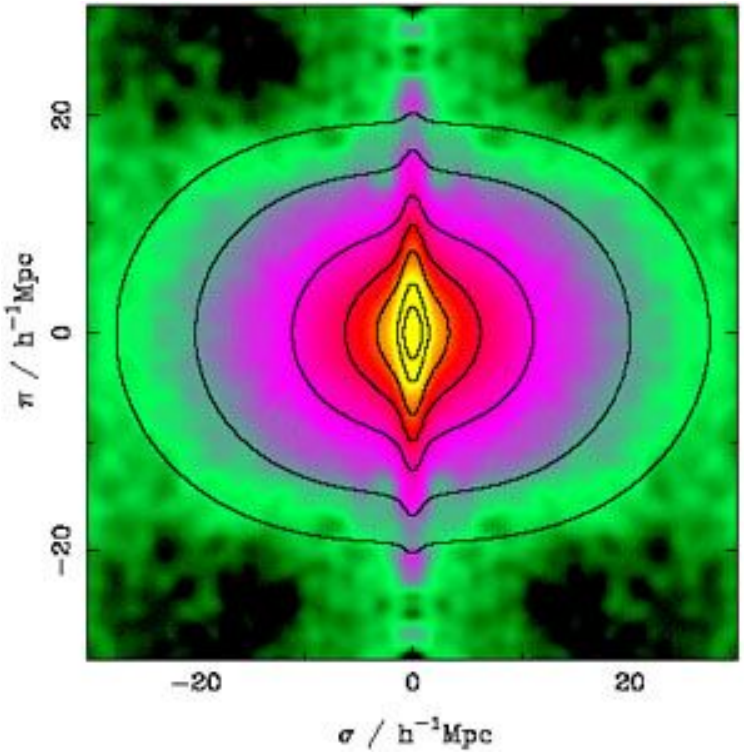


The two-point correlation function obtained from the 2dFGRS by Hawkins et al. (2003). Note the anisotropies due to Finger-of-God and Kaiser effect

# REDSHIFT SPACE DISTORTIONS

**It can be shown that (in linear theory):**

$$\delta_s(\vec{k}) = (1 + \beta\mu^2)\delta_r(\vec{k})$$

$$P_s(k) = (1 + \beta\mu^2)^2 P_r(\vec{k})$$

**Where $\mu$ is the cosine of the angle between the velocity vector and the line of sight and $\beta$ is a function of the linear growth rate, *f*, and tracer bias, *b*:**

$$\beta = \frac{f(\Omega_m)}{b}$$

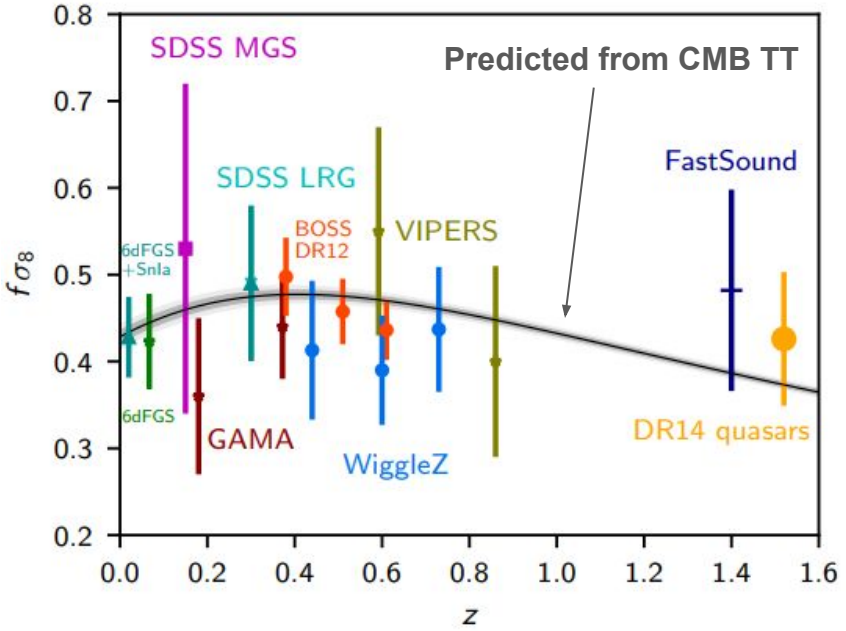


**Thus we can use RSD to constrain the growth of structure over cosmic time.**

# THE KINEMATIC SZ EFFECT

**The kinematic SZ (kSZ) effect is due to the bulk velocity of the ICM electrons slightly changing the apparent temperature of the CMB black body spectrum.**

- **Amplitude of the pairwise kSZ signal:**

$$T_{\rm pkSZ}(r) \equiv \bar{\tau}_e \frac{v_{12}(r)}{c} T_{\rm CMB}$$

$$v_{12}(r,a) \approx -\frac{2}{3} aH(a) f(a) r \frac{b\bar{\xi}(r)}{1+b^2\xi(r)}$$

**ξ(r): Two-point matter correlation function**
**f(a): Growth rate**

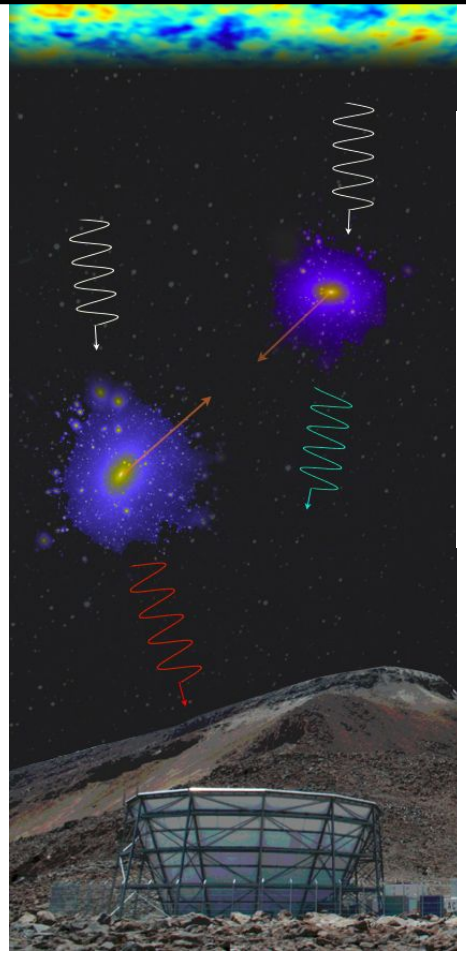

**The pkSZ measured from DESI GC and Planck CMB map (Chen+21)**

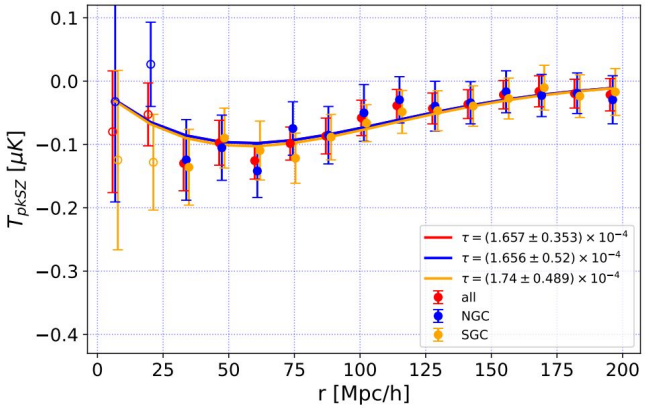


See also: **Roper+25**
**Mass dependence of halo baryon fractions from the kinetic Sunyaev–Zeldovich effect**